Eva-Maria Ölweiner, BSc

Optical continuous blood pressure estimation using machine learning

Master's Thesis
to achieve the university degree of
Master of Science
Master's degree programme: Biomedical Engeneering

submitted to

Graz University of Technology

Supervisor
Dipl-Ing. Andreas Lesch, BSc

Institute for Medical Engineering
Head: Univ.-Prof. Dipl-Ing. Dr.techn. Rudolf Stollberger

Graz, May 2019

This document is set in Palatino, compiled with pdfLaTeX2e and Biber.

The LaTeX template from Karl Voit is based on KOMA script and can be found online: https://github.com/novoid/LaTeX-KOMA-template

Affidavit

I declare that I have authored this thesis independently, that I have not used other than the declared sources/resources, and that I have explicitly indicated all material which has been quoted either literally or by content from the sources used. The text document uploaded to TUGRAZonline is identical to the present master's thesis.

Date	Signature

Abstract

This master thesis deals with the continuous estimation of blood pressure by an artificial neural network from a plethysmographic signal of an optical sensor. For the training of the artificial neural network, single heart cycles are extracted from the filtered and processed measurement data and then decomposed into complex frequency components using a fast Fourier transformation algorithm. These components are used as input variables for the neural network with three hidden layers. Two different data sources are used to train the network. On the one hand a public database (MIMIC) that provides optical signals from the fingertips of test persons and on the other hand own measurements with an optical PALS-2 sensor at the wrist of the test persons. An invasive blood pressure measurement is used as a reference measurement for the MIMIC database and the continuous, non-invasive method according to Peňáz is used for the self-acquired data.

The work has shown that it is possible to determine the blood pressure from the photoplethysmographic signal of test persons if data with similar characteristics are available in the training data set. This is best given within a homogeneous group of subjects. Whether it is ultimately also possible to determine blood pressure from a photopletysmographic signal in elderly persons and for pathological changes through a very large reference database cannot yet be answered.

Keywords: blood pressure, photoplethysmography, FFT-features, machine learning, neuronal network

Kurzfassung

Diese Masterarbeit beschäftigt sich mit der kontinuierlichen Blutdruckschätzung durch ein künstliches neuronales Netzwerk aus einem photoplethysmographischen Signal eines optischen Sensors. Für das Training des künstlichen neuronalen Netzwerkes werden aus den gefilterten und aufbereiteten Messdaten Einzelherzzyklen extrahiert die anschließend mit einem Fast-Fourier-Transformations-Algorithmus in komplexe Frequenzkomponenten zerlegt werden. Diese Komponenten werden als Eingangsgröße für das neuronale Netzwerk mit drei versteckten Schichten verwendet. Für das Training des Netzwerkes werden zwei unterschiedliche Datenquellen herangezogen. Einerseits eine öffentliche Datenbank (MIMIC) die optische Signale von den Fingerspitzen von Probanden zur Verfügung stellt und anderseits eigene Messungen mit einem optischen PALS-2 Sensoren am Handgelenk der Probanden. Als Referenzmessung wird für die Datenbank MIMIC eine invasive Blutdruckmessung und für die selbst akquirierten Daten die kontinuierliche, nichtinvasive Methode nach Peňáz verwendet.

Die Arbeit hat gezeigt, dass die Möglichkeit besteht, den Blutdruck aus dem photoplethysmographischen Signal von Probanden zu ermitteln, wenn Daten mit ähnlichen Eigenschaften in den Trainingsdaten vorhanden sind. Dies ist am besten innerhalb einer homogenen Gruppe von Probanden gegeben. Ob es letztlich auch möglich ist durch eine sehr große Referenzdatenbank, bei älteren Personen und pathologischen Veränderungen den Blutdruck aus einem photopletysmographischen Signal zu bestimmen kann noch nicht beantwortet werden.

Schlüsselwörter: Blutdruck, Photoplethysmographie, FFT-Features, maschinelles Lernen, neuronales Netzwerk

Contents

Acronyms

ANN artificial neural network. 2, 45, 55
ASR artefact to signal ratio. 20

BP blood pressure. 2–4, 10, 11, 13, 27, 28, 30–32, 38, 39, 41, 44–46, 67, 68, 76, 81, 82, 92
BPV blood-pressure variability. 13, 14

ECG electrocardiogram. 8, 9
EEG electroencephalography. 61

FFT fast Fourier transformation. 6, 32, 43–45, 55, 56, 60, 62, 67, 81, 85, 87–89, 94
FWHM full width at half maximum. 22

HID human interface device. 37, 43

MSE mean squared error. 41, 55, 57, 59

PPG photoplethysmography. 2, 4, 17–20, 22, 24, 26, 27, 31, 32, 35, 38–46, 48, 55, 60, 62, 72, 80, 85, 92, 94, 95
PTT pulse transit time. 28–30

RMSE root mean squared error. 67

USB universal serial bus. 37

1. Introduction

1.1. Motivation

Arterial blood pressure is a very important vital parameter in the diagnosis of cardio vascular diseases like myocardial infarction or heart failure, and to observe their treatment success [1]. Currently several methods exist to measure the arterial blood pressure noninvasively, like using the Korotkoff sounds, the oscillometric method [2] or the method of Peňáz [3]. The Korotkoff and oscillometric method are easy to implement and the technical effort is very low and cheap. However, these methods require to inflate and deflate the cuff, which interrupts the arterial blood flow. This interruption heavily influences the cardio vascular system, making a certain recovery phase necessary before the measurement can be repeated. It is recommended to keep the measurement interval smaller than two minutes to achieve reliable results [4]. Contrary to that, the Peňáz method allows a continuous measurement using a regulation circuit to achieve a constant extremities blood volume. However, the technical effort for this method is quite high, including the oscillometric reference measurement. This is limiting the applicability to stationary measurements like in an intensive care unit and the cardio vascular system is also influenced by the measurement. For some diseases a continuous measurement of the arterial blood pressure is desirable during activity, sleep or simply for a long term observation in daily routine. Using the existing methods this can be done until a certain degree, however due to the measurement principles it can be very disturbing for the patient especially during physical activity and sleep. Additionally the interest on wearable devices and fitness tracking is rising based on the need to control the state of health and for workout monitoring. By measuring the blood pressure at a medical appointment, the behaviour of the patient changes and this leads to a change of his bio-signals. This phenomenon is called the

‚white coat effect' which leads to increased blood pressure due to the nervousness during medical examinations. A more descriptive term for the cardiac behaviour is home measured data which avoids this effect [5]. BP monitoring systems for easy self-measurement may benefit patients by providing information about the effect of antihypertensive medication. The higher the BP, the higher the risk for cardiovascular disease, for example myocardial infarction, heart failure, stroke and other risks like kidney disease [1].

The target of this thesis is to investigate whether it is possible to use the measurements of the optical PALS-2 sensor for non-invasive continuous blood pressure measurement. This method is based on an optical absorption measurement where the signal is inverse proportional to the arterial blood volume (Photoplethysmography (PPG)). The shape of this curve changes with blood pressure according to the arterial wall stiffness as described in [6] and additionally depends on many physical and biological factors. This effect is exploited to estimate the systolic and diastolic blood pressure using a neural network.

1.2. Previous work and defined scope

This thesis is based on a previous work [7] with promising results. In the previous work individualized models were trained. This means that an unique training process has to be done for each individual. The achieved weights and biases of the artificial neural network (ANN) are only trained for this specific person. PPG data provided by the MIMIC database and self measured data by using the Infineon Opto ASIC PALS-2 were used as basis for the blood pressure (BP) estimation. The work showed that the principle of blood pressure estimation using photoplethysmograpic data can work, however the result should be viewed critically, because of the very small dataset used. 30 samples were used to train the neural network and the cycles were selected manually for the self-measured data. Only a few minutes per individual were extracted from the database and used for training and testing the neural network. This leads to a very low data variability and a small range of blood pressure values.

The following section summarizes the predefined scope of this work.

a. State of the art for continuous blood pressure measurements
Literature research concerning possible modern methods for continuous BP measurement should be done.

b. Arterial wall mechanics
Providing knowledge concerning the physiological background and how the blood pressure shape is merged and affected.

c. Sensor communication and data tracking environment
Development of an environment for easy sensor communication, data tracking and data saving.

d. Confirmation or disproof of the main principle
The principle of blood pressure estimation using photoplethysmographic signals should be investigated.

e. Expansion of the dataset
If part d. is proven to be possible, the dataset should be expanded for getting a wider range of data and people.

f. Generalized method of blood pressure estimation
Examinations concerning the possibility to achieve a general neural network for estimating blood pressure for different individuals should be performed.

The system should be developed in Python, an open source programming language including packages for deep learning and signal processing.

1.3. Overview of the thesis

The aim of this thesis is to estimate a persons blood pressure from his photoplethysmographic measured signals. The general part describes the underlaying physiological mechanisms followed by engineering fundamentals, including the principle of the PPG measurement and a description of other reasonable non-invasive BP measurement methods as well literature research concerning pressure estimation using artificial neural networks. The PPG data quality is strongly varying for measurements and patients due to different sensor positions, movements and person-specific influences like skin color, the surface temperature of the skin, persons weight and circulation. Due to that, the assessment of signal quality plays an important role for reliable results. Figure 1.1 gives a short summary of the implemented solution. After preprocessing, individual heart cycles are cut out from the continuous measured signal. Due to different heart cycle lengths it is necessary to zero-pad the single cycles to a predefined length, then each is Fourier-transformed. Both, amplitude and phase information describe the shape of the PPG heart cycle and thus is fed into the neuronal network. The network is trained using BP data which were synchronously measured with the PPG signal. Two different data sources were used for the investigations: Data were provided on the MIMIC database [8] including PPG signals measured on the fingertip combined with invasive BP measurement. The self measured data were gained using the Infineon Opto ASIC PALS-2 for PPG signal acquisition. A reference signal is acquired using the Task Force Monitor (V2.3.20, CNSystems, Graz, AUT).

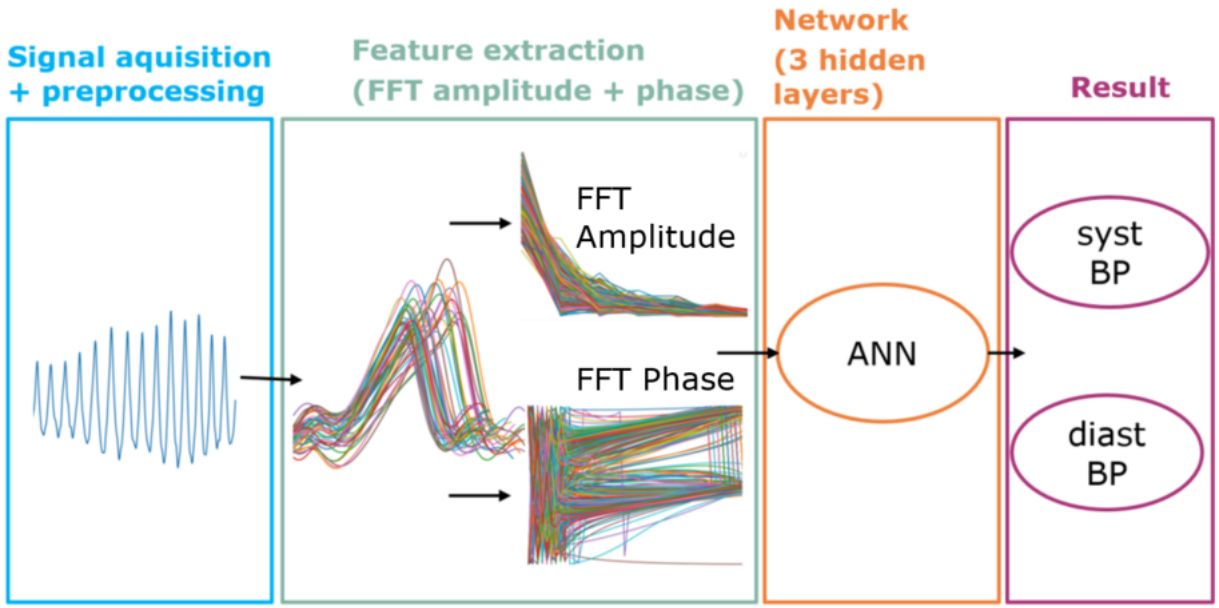

Figure 1.1.: Overview of the signal-processing flow; Individual cycles, cut out from the whole signal, are Fourier-transformed and passed to the neural network (as features). After training, the network estimates a systolic and diastolic blood pressure value

Different scenarios regarding the feature extraction and datasets were investigated. The following list gives an short overview about the different performed experiments:

1. **Database; FFT; Test persons included in trainingsset**
   The fast Fourier transformation (FFT) was performed on single heart cycles gained from the database data. The single heart cycles were split into a train and a test set; cycles of each individual were included in both train and test set.
2. **Szenario 1. with additional windowing**
   After the extraction of single heart cycles out of the continuous signal, windowing was performed at each cycle. The calculation of the features, the data used and the distribution of the train and test set corresponds to the previous scenario.
3. **Database; FFT; Test persons excluded from trainingsset**
   As descibed in 1. the FFT was performed on single heart cycles gained from the database data. The individuals were split into train- and test-persons. In this case heart cycles of the test-persons were not included in the training set.
4. **Self-measured data; FFT; Test persons included in trainingsset**
   The FFT was performed on single heart cycles gained from the self-measured data. The single heart cycles were split into train and test set; cycles of each individual were included in both train and test set.
5. **Self-measured data; FFT; Test persons excluded from trainingsset**
   As described in 4. the FFT was performed on single heart cycles of the self-measured data. The dataset was splitted as described in 3: Heart cycles of individuals included in the training set were not used in the test set and vice versa. Since all available persons were used to train the network, additional measurements were performed to obtain test data from other people.
6. **Database; Wavelet; Test persons included in trainingsset**
   To investigate the possibilities of Wavelets, the Wavelet transformation was performed on single heart cycles gained from the database data. The single heart cycles were split into train- and test-set; cycles of each individual were included in both train and test set.

2. Physiological background

2.1. Blood flow and pressure in the arterial system

At contraction during the systole of the heart beat the pressure in the left ventricle rises steeply, until it exceeds the internal aortic pressure. A pressure gradient between the aorta and ventricle is generated, this leads to the opening of the aortic valve. Now the blood moves with rapidly increasing flow into the ascending aorta until the flow maximum appears, afterwards the flow decreases back to zero. During the closing of the aortic valve a small amount of blood flows back into the heart. This causes a momentary negative blood flow and a pressure drop. At the beginning of the following diastole, the blood flow in the aorta remains zero, the blood stands still and the aortic valve is closed because the pressure in left ventricle is smaller than in the aorta. At the beginning of the next systole the aortic valve opens again and the heart cycle starts from beginning. The insertion of blood into the aorta is done by a rhythmical blood flow pulse. In most cases the duration between two pulses is longer than the pulse itself. [9]

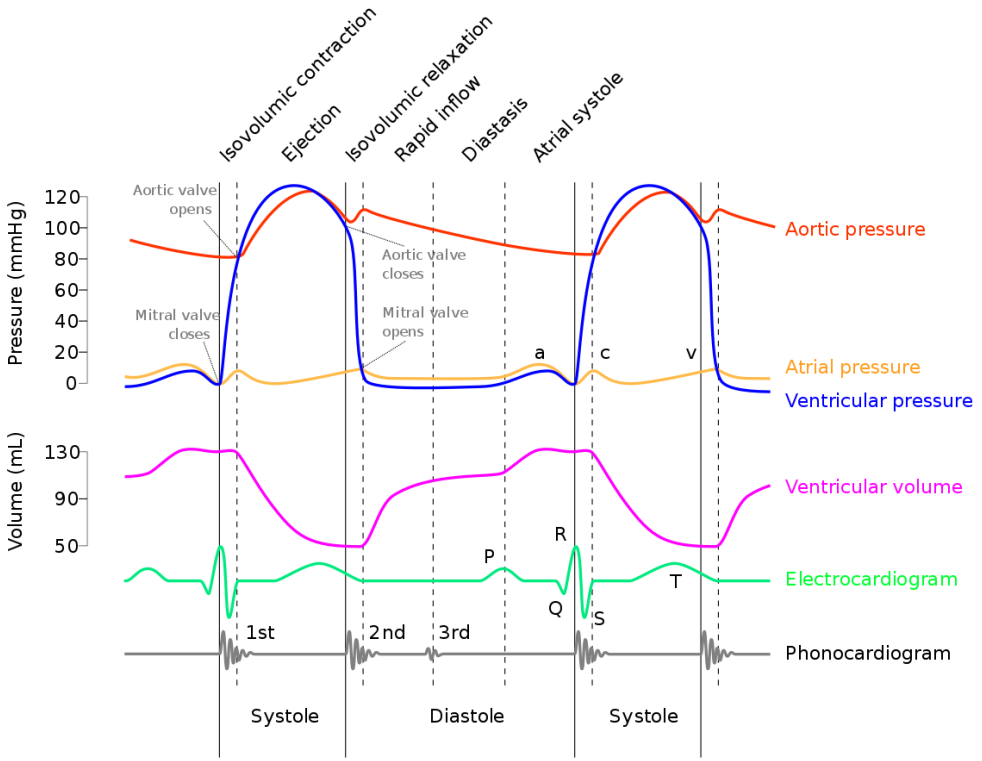

Figure 2.1.: Pressure an volume plot of the heart; The aortic, atrial and ventricular pressure in the left ventricle are shown over time on the top of the Figure. Additionally, the corresponding ventricular volume, the ECG signal and the Phonocardiogramare are shown over two heart periods [10].

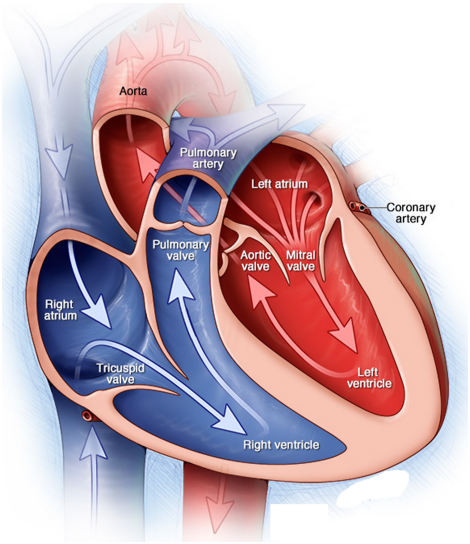

Figure 2.2.: Internal heart structure including the direction of blood flow; On the right side the left ventricle delimited by the mitral valve and the aortic valve is pictured [11].

The time course of the aortic and ventricular blood pressure as well as the corresponding ventricular volume are shown in Figure 2.1 over two heart periods compared to the ECG signal and the Phonocardiogram [10]. Figure 2.2 shows the internal heart structure including the direction of the blood flow [11].

2.2. Winkessel function of the elastic arteries

At each systole a blood volume of about 70 - 140 ml is ejected into the arterial system. This leads to rhythmical volume fluctuations which do not directly continue into the arterial system. During the ejection period of the heart the aorta and vessels near to the heart, store one part of the ejected volume. Due to their elastic properties they are able to increase their volume. When the internal pressure decreases during the diastole, the stored blood is delivered to adjacent vessels. This mechanism is called the Windkessel function and ensures that the blood is pumped roughly continuously through the arteries despite rhythmical heart activity. [12]

During the systole about 50% of the stroke volume is stored in vessels near the heart and distributed during the diastole. The flow energy is converted into potential energy of the elastic stretched arteries. At the diastole it is converted into kinetic energy. This effect leads to a relief of the heart because the transport of a balanced flowing blood mass requires less effort for acceleration. [12]

Figure 2.3 shows the difference of the Windkessel function between elastic and stiff arteries [13].

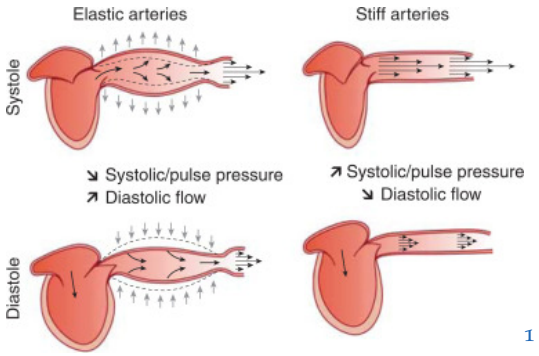

Figure 2.3.: Winkessel function for elastic and stiff arteries; Elastic vessels are able to store blood volume during the systole and increase therefore the diastolic flow. In contrast, less blood is stored by stiff arteries what leads to an increase of the systolic pressure and a decrease of the diastolic flow [13].

2.3. Blood pressure wave propagation

The BP wave is generated as described in Chapter 2.1. It travels through the arteries and is reflected multiple times. The reflection of the pulse wave is caused at the branches of the aorta. The resulting pressure waveform is the sum out of the forward travelling wave and the reflected, back travelling wave. The back travelling wave can be interpreted as an echo of the incident wave. The waveform depends on the mechanical properties of the arteries. Due to the mechanical characteristics of the arteries, the timing and also the magnitude of the incident and reflected waves can change. In case the main arteries are healthy and elastic, the diastolic blood pressure is increased. The reason is that the reflected wave merges

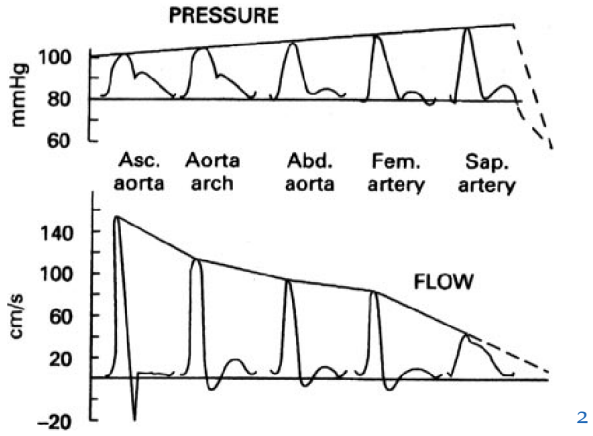

Figure 2.4.: Change of the pressure waves shape along the arterial tree [14]

witch the incident wave during the diastole in the proximal aorta. In case of stiff arteries, the velocity of the pulse wave increases and the incident and reflected wave merge at the systole, so that the aortic systolic pressure is increased.[14]

An important point regarding the relationship between the brachial and the central aortic pressure is the effect of pressure wave amplification. The value of the diastolic BP changes little across the arterial tree, the mean BP sinks slightly. The value of the systolic BP is increased in more peripheral regions shown in Figure 2.4. The pulsatile components of the systolic BP and pulse pressure (PP) can vary greatly. In general brachial systolic BP measurements tend to overestimate the central systolic blood pressure. [14]

2.4. Blood pressure regulation system

The simplified BP regulation system can be shown as a typical regulation loop. The mean arterial pressure depends on the product of the peripheral flow resistance and the cardiac output. A drop in blood pressure can be counteracted by increasing the cardiac output or the peripheral resistance. Pressure should be kept at a specific level and can be seen as the control variable of the regulation system. Baroreceptors, located at four areas in

the arterial system, are placed in the vessel's wall for determining the actual pressure. The sinus caroticus (a vessel dilation at the beginning of the internal carotic artery) and the aortic depressor nerve act as stretch receptors. The advantage compared to the usage of pressure receptors arises from the non-linearity of the vessels wall stretching curve. The counter regulation of the system is even stronger the lower the pressure is. For the same pressure change, the change of the corresponding stretch value is not linear for high and low pressures. In case of low pressures, the stretch change is much higher than at high pressures. The information about the actual stretch of the arteries is processed in the circulatory center of the central nervous system. [9]

The higher the stretch and the faster the arteries are stretched the higher is the pulse density of the action potential. This results in an excitement of the nervus vagus (the tenth cranial nerve) proportional to the stretch of the arteries. The nervous vagus is involved in the regulation of the activity of almost all internal organs and the largest nerve of the parasympathetic system. The nervous vagus regulates the vasoconstriction, by changing the Windkessel and the peripheral vascular resistance, the stroke volume and the pulse rate are decreased. [9]

In case of drop of the arterial stretch the sympathetic nerves are activated. The vasoconstriction and the heart muscles frequency is increased (mainly by the release of noradrenaline). Additionally, the vessel's tonus and peripheral resistance are increased. The effect of the vasoconstriction is applied rapidly but has a fleeting effect. In addition, adrenaline is released in the bloodstream and stimulates with a persistent effect the heart and the vasomotoric center. Also the blood reservoir, the veins, the liver and the spleen are stimulated and they increase the blood volume and therefore the mean arterial strain. [9]

Figure 2.5 illustrates the described regulatory system. The system behaves in analogy to an electrical circuit and follows Ohm's law. This topic is treated in Chapter 3.2. Other influences of this regulation systems are the thermoregulation of the hypothalamus, ascendancies of the diencephalon(limbic system) and telencephalon (worries) [9]. This Chapter cannot accurately describe the whole scope of acting influences and should only give a short overview about this topic.

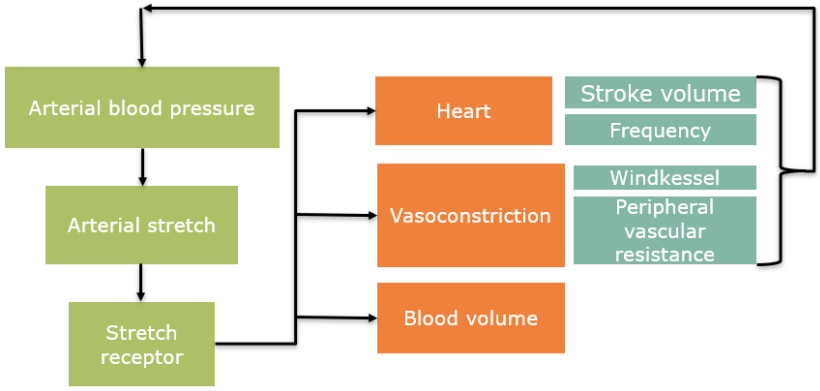

Figure 2.5.: Overview of BP regulation system; The arterial strech is related to the arterial blood pressure and measured by stretch receptors. The stroke volume of the heart, the heart frequency, the vasoconstriction and the blood volume are regulated to influence the arterial pressure.

2.5. Classification of blood pressure

The lowest value in the blood pressure curve is normally reached at the beginning of every pulse, that means at the end of the diastole. It is called the ‚diastolic pressure' and has a value of about 80 mmHg (10.7 kPa). The peak value is reached in the systole and is called ‚systolic pressure', normally reaching about at 120 mmHg (16.0 kPa). [9]

Table 2.1 shows how BP is classified. The personal blood pressure is strongly related to everybody's lifestyle. To prevent cardiovascular risks by decreasing hypertension, lifestyle modifications such as weight reduction and moderation of alcohol consumption can achieve good results. For example a weight loss of 10kg leads in average to an approximately systolic BP reduction of 5 -20 mmHg. [1]

2.6. Variability of blood pressure

Blood pressure is a variable haemodynamic phenomenon that is influenced by many factors, also by the measurement itself. The blood-pressure variability (BPV) includes short term fluctuations occurring within a 24 h

Table 2.1.: Classification of blood pressure for adults aged 18 years or older [1]

BP classification	Systolic BP		Diastolic BP
	mmHg		mmHg
Normal	< 120	and	< 80
Prehypertension	120 - 139	or	80 - 89
Stage 1 hypertension	140 - 159	or	90 - 99
Stage 2 hypertension	$\geq$ 160	or	$\geq$ 100

period and changes over more-prolonged time periods with different underlying mechanisms. Very short term BPV can only be measured by beat-to-beat measurements over time. BPV can be divided into the following types: [15]

Very short-term BPV (beat-by-beat)
Short-term BPV (within 24h)
Long-term BPV (day-by-day)
Very long-term BPV (visit-to-visity)

The BPV analysis gives an insight into the central sympathetic drive, humoral and rheological factors, behavioral and emotional factors, activity/sleep and ventilation [15]. Figure 2.6 shows a typical blood pressure progression. It shows that the beat-by-beat variations are in the range of 5 mmHg.

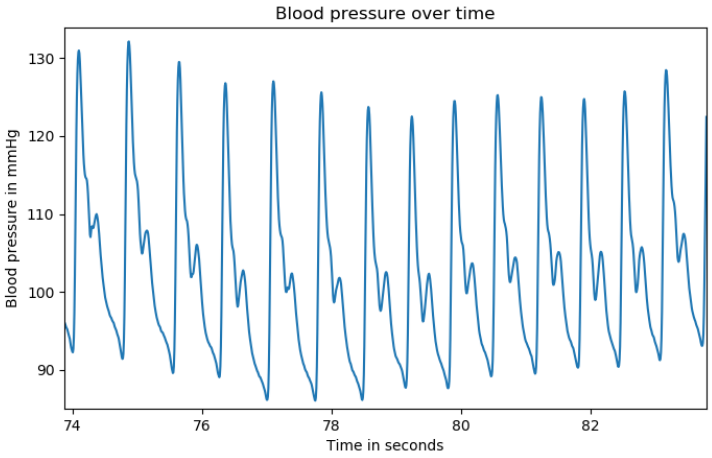

Figure 2.6.: Short term blood pressure variability; Beat-to-beat variations are in the range of 5 mmHg; Measured by using the Task Force Monitor.

3. Medical engineering fundamentals

3.1. Photoplethysmography

Photoplethysmography is an optical technique for non-invasive blood volume change estimation. This is done by lighting up tissue and measuring the reflected or transmitted light. This signal is widely used for heart rate and oxygen saturation measurements. [16]

The main principle of PPG signal acquisition is shown in Figure 3.1. The variation of the blood volume is caused by the pulsation of blood pressure over the cardiac cycle. Depending on the current pressure the diameter of the arteries is more or less dilated and the amount of blood changes. This thesis is based on a measurement based on the backscattering of green light located on the wrist. The wrist was chosen as measuring point because of possible further applications in commercial wrist watches.

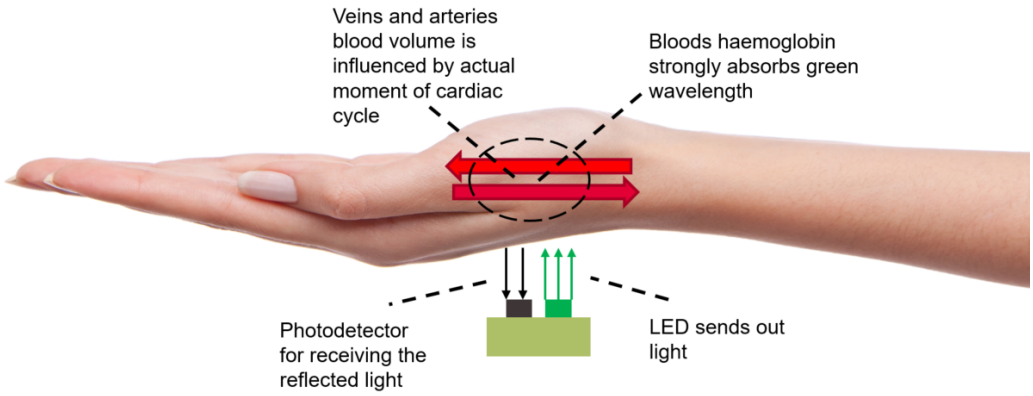

Figure 3.1.: Overview of PPG signal acquisition [17]

The PPG signal is composed of a pulsatile part (AC) and a slowly varying DC baseline. The DC baseline is manly affected by various lower frequency components attributed to the sympathetic nervous system activity, respiration and thermo-regulation. The AC part is attributed to cardiac synchronous changes in the blood volume of each heart beat, and has its fundamental frequency typically around 1 Hz according to the pulse rate. The quasi-DC component superimposes the AC part and relates to the tissues and the average blood volume. It is slowly variated due to respiration, vasomotor activity, vasoconstrictor waves, Traube Hering Mayer (THM) waves and also thermo-regulation. Various optical effects as scattering, absorption, reflection, transmission and fluorescence are included by light interaction with biological tissue. The amount of detected light by the photodetector can be related on the following key factors: blood volume, blood vessel wall movement and the orientation of the red blood cells. [18]

3.1.1. Wavelength selection

Three main reasons are important for the selection of the wavelength for the optical radiation: The optical water window, the isobestic wavelength and the tissue penetration depth [18]. The absorption spectrum of water and other biological tissues is shown in Figure 3.2.

The optical water window Water is the main constituent of the human tissue. Light at longer infrared and ultraviolet wavelengths is absorbed very strongly by water, melanin absorbs stronger at shorter wavelengths. The wavelength range with minimal absorption in the human tissue is called the optical water window. [18]
This window in the near- infrared region defines the range between 650 to 1350 nm.

Isobestic wavelength The absorption between oxyhaemoglobin (HbO_2) and desoxyhaemoglobin (Hb) shows a significant difference, except at the isobestic wavelength located at 805 nm. When measurements use the isobestic wavelength, the signal should be unaffected by changes in the blood oxygen saturation. [18]

Tissue penetration depth The penetration depth is the depth of light at which the light intensity drops by $1/e$ and depends strongly on the

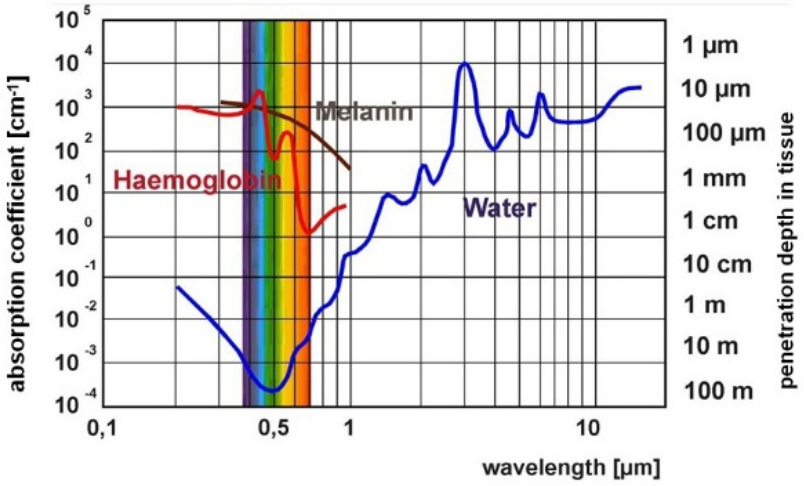

Figure 3.2.: Absorption spectra of water, melanin and haemoglobin at different wavelengths [19].

used wavelength [18]. The optical penetration depth for blue, green and infrared light is shown in Figure 3.3.

[16] suggests that green light is more suitable for wrist sensor applications than blue or infra-red light. Green and blue light penetrates less than infra-red light. This is the reason why PPG signals measured with short wavelengths are less influenced by movements located in the deeper tissue. The skin penetration depth of light is shown in Figure 3.3. The optical penetration depth calculation can be performed using absorption and scattering coefficient of the tissue and is given with Equation 3.1. [16]

$$\delta(\lambda) = \frac{1}{\sqrt{3 \cdot \mu_a(\lambda) \cdot (\mu_a(\lambda) + \mu_s(\lambda))}} \tag{3.1}$$

Where δ is the penetration depth in mm, μ_a is the absorption coefficient in mm^{-1} and μ_s is the scattering coefficient in mm^{-1} [16].

Figure 3.4 compares the PPG response at three different wavelengths: blue (465 nm), green (520 nm) and infrared (940 nm) and at different light intensities: 1.28 mW/sr, 0.82 mW/sr and 0.26 mW/sr. The measurements were done on the wrist using normalized radiant intensities. Artifacts

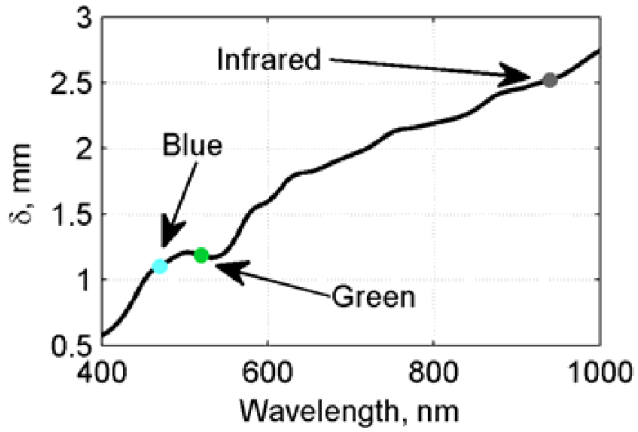

Figure 3.3.: Optical penetration depth vs. wavelength of light [16]

were induced in the middle of the recordings by tapping the PPG sensor three times in a row. Each experiment was repeated tree times. Three criteria were investigated: the root mean square value of the PPG signal before the artifact, pulsation to stationary component ratio (AC/DC) and artefact to signal ratio (ASR). The ASR was calculated with the following equation: [16]

$$ASR = \frac{V_a}{V_{PPG}} \tag{3.2}$$

where ASR is the artefact to signal ratio, V_a is the magnitude of the PPG signal during tapping the sensor and V_{PPG} is the average amplitude of the PPG signal 20 seconds before the artefact [16].

It is shown that green light has the highest RMS, the lowest ASR and the highest AC/DC values when using on the wrist. This shows that using green light at wrist PPG application is more suitable than blue or infrared light. It penetrates deep enough to sense blood pulsations and it is less influenced by the DC part of the tissue. [16]

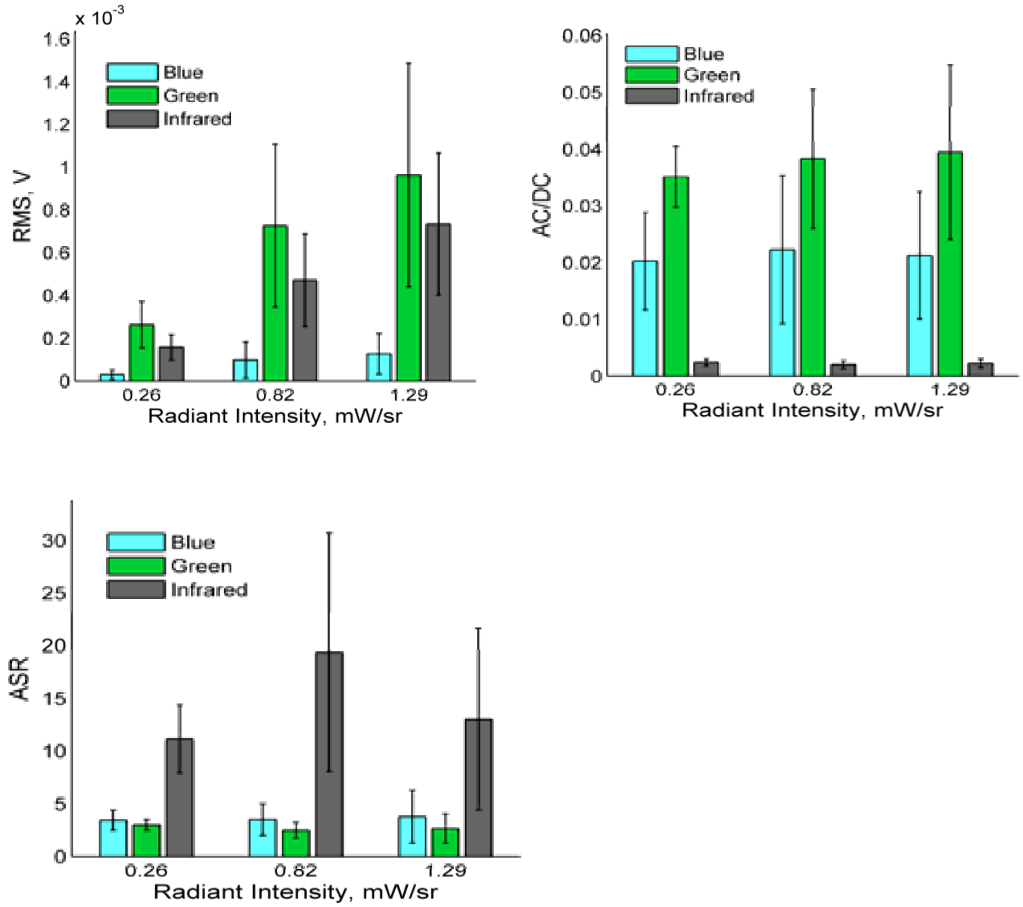

Figure 3.4.: Left top: RMS value of the PPG signal as the function of light intensity measured on the wrist; Right top: AC/DC ration at the function of light intensity measured on the wrist; Bottom: Artifact to signal ratio as the function of light intensity measured on the wrist [16]

3.1.2. Instrumentation

The main components of PPG instrumentation are the light source (LED) and a matched photodetector. LEDs have a long operation life ($> 10^5$ h) and a narrow bandwidth (the full width at half maximum (FWHM) is about 24 - 27 nm). They are compact, mechanically robust and they operate over a wide temperature range. The LEDs averaged intensity should be constant. The photodetector and its characteristics are chosen to match those of the light source and converts the light energy into electrical current. Usually it is sensitive, low-cost and compact. The photodetector is typically connected to an transimpedance amplifier circuit followed by an filtering circuit. [18]

Figure 3.5 show the electronic building blocks used for PPG measurements. Figure 3.6 shows a typical transimpedance amplifier.

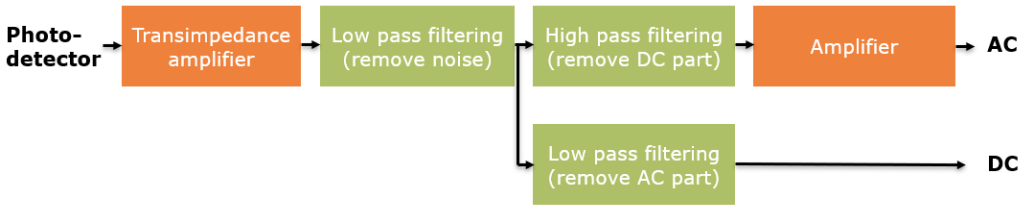

Figure 3.5.: Typical arrangement of the electronic building blocks used for PPG measurements. The transimpedance amplifier is followed by a low-pass against the noise and a high-pass against the DC part. The AC part is amplified and the preprocessed signal can be used for further processing.

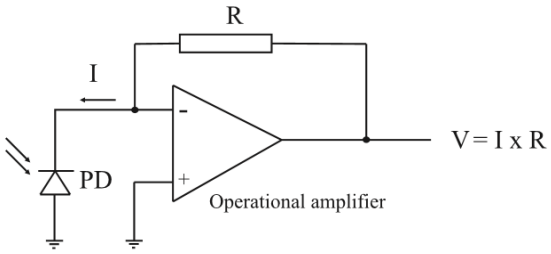

Figure 3.6.: The light intensity which hits the photodiode is converted into an amplifier output voltage by a transimpedance amplifier stage [18].

3.2. Relation between pressure, flow and resistance: The omic law

This Chapter should give an overview about the cardiovascular relations of blood pressure, blood flow and body internal flow resistance. The arterial and venous system of the human body can be described by arterial and venous compartments and flow resistance. The different compartments are separated by a flow resistance and described by a compliance element. This compliance element is given by the inverse elasticity of the vessels. The major resistance to flow is located in the peripheral regions between the arteries and veins. The flow resistance of large vessels is small in comparison to the resistance of peripheral vessels. In analogy to electrical systems, blood pressure plays the role of voltage and volumetric flow the role of current. In the described model it is assumed that the diameter of the middle cerebral arteries remains constant. Measurements of the middle cerebral blood flow have shown that the blood velocity in this vessel can be seen as constant despite big changes of the diameter because of different biological stimuli. The assumption is based on the volume conservation law. By calculating the volume and volume change in each compartment blood pressure and volumetric blood flow can be found. Equations for the arterial and venous compartments are similar. Equation 3.3 shows how the volume at each cardiac cycle is calculated. [20]

$$V_{stroke} = Cp \tag{3.3}$$

Where V_{stroke} is the volume pumped out during one cardiac cycle in cm^3, C is the Compliance in $cm^3/mmHg$ and p in mmHg references the blood pressure. Out of the volume per heartbeat the cardiac output can be calculated. [20]

$$\mathrm{CO} = HV_{stroke} \tag{3.4}$$

Where CO is the cardiac output in cm^3/s, H is the heart rate in beats/s and V_{stroke} gives the volume of each stroke [20]. The change of the volume V of each compartment can be described by Equation 3.5.

$$\frac{dV}{dt} = q_{in} - q_{out} \tag{3.5}$$

$$q = \frac{p_{in} - p_{out}}{R} \tag{3.6}$$

Where q_{in} and q_{out} in cm^3/s are referred to Kirchhoff's current law. R is the flow resistance. Based on Kirchhoff the compartments can be seen as nodes. Many compartments own more than one inflow and outflow. As an example the vena cava has three inflows. [20]

3.3. Mechanics of the arterial wall

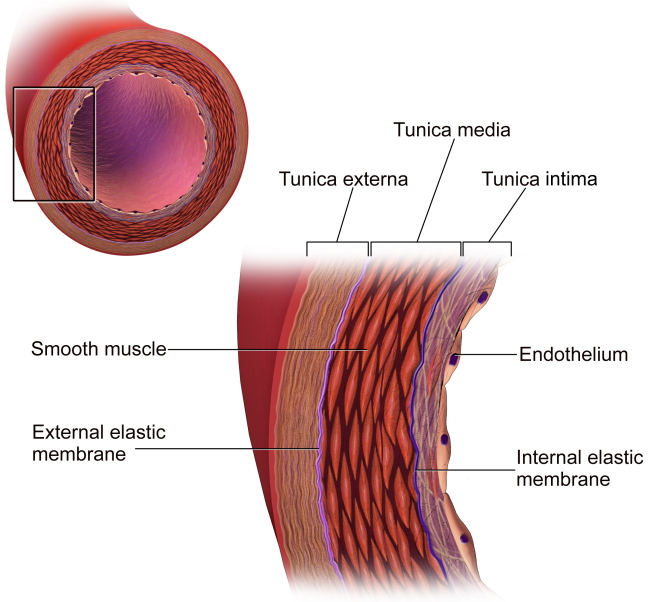

Figure 3.7.: Structure of the arterial wall [21]

The elastic properties of the blood vessels are decisive for the relationship between the internal blood pressure and the PPG signal. Due to the anisotropic composition of the arterial wall and the resulting non-linear elasticity of the blood vessels, simply applying the Hook's law would not adequately describe the vessels behaviour at a changing blood volume. Figure 3.7 shows that the arterial wall consists of three layers, the tunica

intima, tunica media and tunica externa, which contain collagenous and elastic fibres as well as muscle cells. Collagen, elastin and smooth muscle cells are mainly involved in the generation of stress in the arterial wall. The stiffness is generally described with the Youngs modulus E. E is a mechanical property describing the relationship between stress and strain of a specific material. The elastic behaviour of the arterial wall, can be approximated by Equation 3.7 using a combined modulus. The Equation gives an relation between E and the transmural pressure p. The transmural pressure gives the difference of pressure inside and outside of the vessels wall. [6]

$$E(p) = E_0 e^{\gamma p} \tag{3.7}$$

Where E_0 is expressed in Pa and the factor γ in mmHg^{-1} depends on the measuring site and the species, which is an empirical determined factor. γ is in the range of $10 \cdot 10^{-3}\,\text{mmHg}^{-1}$. Equation 3.8 describes the elasticity in dependence of the pressure p, Poisson's ratio σ, the arterial wall thickness h and the mean radius of the blood vessel r. [6]

$$E = (1 - \sigma^2) \cdot \frac{r^2}{h} \cdot \frac{dp}{dr} \tag{3.8}$$

For the blood pressure estimation, the circumferential stress is the most important stress, the conclusion is that E represents the tension-strain modulus and σ can be set to zero [6].

3.3.1. Mathematical modelling of the photoplethysmographic signal

For achieving a simple mathematical model for the PPG signal, it is assumed in [6] that the amplitude of the PPG signal is proportional to the blood volume in the vessels. The volume in the vessels can be descried with Equation 3.9, which emanates from a constant vascular radius r. [6]

$$V = k\pi r^2 + V_0 \tag{3.9}$$

In this Equation k can be interpreted as the average of the arterial blood vessel length and is assumed constant, V_0 is added to correct for the cases of micro vascular and venous blood volume. By combining the Equations mentioned in the previous Chapter 3.7, 3.8 and 3.9 and by supposing that V_0 does not pulsate the following equation is derived. [6]

$$V = \frac{k(E_0\gamma h)^2\pi}{(b + e^{\gamma p})^2} \tag{3.10}$$

The constant b is introduced by integration, it is assumed that b is independent of E_0, γ and h. By approximating the Equation by its first Taylor series order, the model describing V, and thereby also the PPG signals amplitude, can be further simplified. The first order is given in 3.11. [6]

$$V \approx \frac{k(E_0\gamma h)^2\pi}{b^2}(1 - \frac{2}{b}e^{-\gamma}p) \tag{3.11}$$

The amplitude of the AC part of the PPG signal is very small compared to the amplitude of the DC part. This leads to a small normalized signal, the normalization is shown in Equation 3.12. [6]

$$PPG_{norm} = \frac{V - V_{min}}{V_{min}} = \frac{2(e^{-\gamma p_{min}} - e^{\gamma p})}{b - 2e^{\gamma p_{min}}} \tag{3.12}$$

The PPG signal is strongly person dependent mainly due to the person related blood vessel elastic properties E. This circumstance makes it difficult to find a model that works for all people to the same extent. Due to the normalization, the signals of different individuals become comparable, because the dependence on E is cancelled out.[6]

3.4. Continuous non-invasive blood pressure measurement methods

3.4.1. Cardiovascular unloading technique

The vascular unloading technique is one of the most basic procedures for continuous non-invasive BP measurements. This widely used method is based on a PPG measurement. Light is illuminating an extremity of the human body containing an artery (e.g., finger, carpus, temple , etc.). The pulsatile blood volume absorbs part of the light, and the reflected or transmitted light is measured by a photo cell (PC). The basic principle can be seen in the original drawing of Peňáz (1973) shown in Figure 3.8.

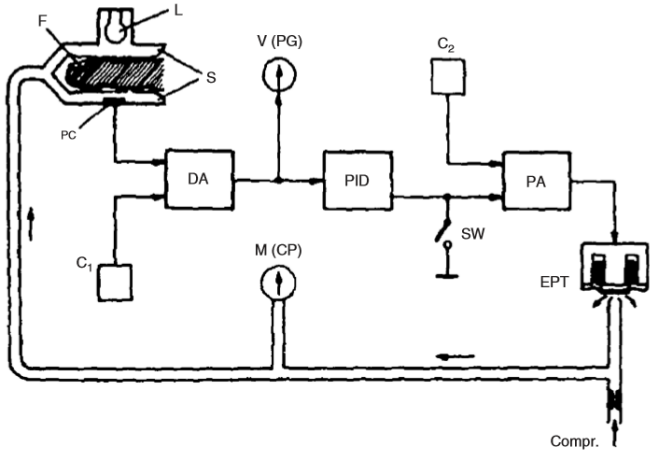

Figure 3.8.: Principe of the Penaz system shown in a block diagram: Lamp (L), Finger (F), photo cell (PC), segments of pressure cuff (S), average of PC-signal (C1), difference amplifier (DA), plethysmographic signal (PG), correcting network (PID), set point (C2), SW switch between open and closed loop, power amplifier (PA), electro-pneumatic transducer (EPT) [3]

The more blood in the arteries the more light is absorbed from the blood and less light encounters the photo cell (PC). C_1 represents the mean value of the PPG signal. A differential amplifier (DA) subtracts C_1 from PC. The result is the PPG signal (PG). PG is used as input of an PID (proportional-integral differential) - controller, the output of the controller

is added to the constant set point C_2. This value is the control size of the electro-pneumatic transducer (EPT). By the EPT a pressure signal $p_c(t)$ in the cuff is produced. This pressure is applied to the finger illuminated by the IR-light. [3]

It should be achieved that PG shall become zero over one cardiac cycle due to the applied pressure $p_c(t)$. During the systolic increasing of the blood volume, $p_c(t)$ is increased until the volume in the finger is decreased. During the diastole the fingers volume is decreased and the system also decreases $p_c(t)$. Because blood volume is held constant over time the intra-arterial pressure p_a is equal to the cuff pressure $p_c(t)$, witch can easily be measured. [3]

The main drawback of this method is, that the system had to be calibrated once via a cuff-based measurement witch may cause deviations between the real blood pressure and the measured. Without this calibration the system can only track the local temporal change in pressure.

3.4.2. Pulse wave velocity method

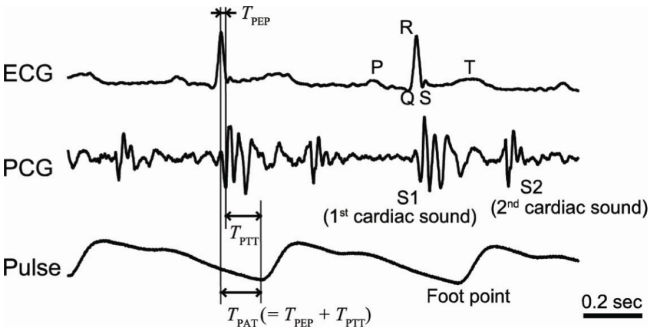

Figure 3.9.: Schematic of the used signals in the pulse velocity calculation. [22] The pulse wave transit time (T_{PTT}) describes the duration of the blood wave propagation through the arterial tree. Alternatively, it can be replaced by the pulse arrival time(T_{PAT}), because of the low variations over time of the pre-ejection period (T_{PEP}). [22]

The pulse wave velocity method is based on the pulse transit time (PTT) which describes the duration for the propagation of the BP wave through the arterial tree. For determining the PTT, biological signals

as shown in Figure 3.9 are analyzed: pulse wave, electrocardiogram and phonocardiogram. Using these signals the pulse wave velocity is calculated. There is an opposite correlation between blood pressure and PTT. Equation 3.13 shows the relationship between the systolic blood pressure p_s and the pulse wave transit time $T_{PTT}(t)$. [22]

$$p_s = \frac{1}{\alpha \cdot ln(2\rho r \Delta x^2 / (E_0 h T_{PTT}^2))} \tag{3.13}$$

The Equation is derived by combining blood vessels elasticity and the Moens-Kortewes Equation, describing the relation between Youngs modulus of the arterial wall E and the speed of the pulse wave. α is a constant related to be blood vessel's characteristics, E_0 is the modulus of longitudinal elasticity of the blood vessel when p_s is 0 mmHg, h is the vascular wall's thickness, ρ is blood density, r is the intra-vascular diameter and Δx the distance between the pulse wave measurement point and the heart. Figure 3.10 shows a picture of the parameters used for blood vessels diameter description. [22]

Equation 3.13 does not take into account changes of the blood vessels diameter and because of that it does not cover a wide range of physiological status from rest to exercise. Due to stress or exercise the blood vessels diameter increases. In Equation 3.14 Δp describes the variation of the intra vascular pressure times the central blood vessels angle $\Delta\theta$. [22]

$$\Delta p r \Delta\theta = 2E\Delta r / r \cdot h sin(\Delta x / 2) \tag{3.14}$$

Where E is the blood vessel's Young modulus of longitudinal elasticity and Δr is the variation of the blood vessel's diameter. By combining Equation 3.13 and 3.14 and after performing several mathematical steps Equation 3.15 is derived. In case of noisy PPG signals it is often not possible to detect $T_{PTT}(t)$ exactly. The variations over time of the pre-ejection period are very small because of that $T_{PTT}(t)$ is replaced by $T_{PAT}(t)$, the pulse arrival time. It is defined as the time between the foot print of the pulse wave signal and the R wave peak event of the electrocardiogram. [22]

$$p_s = \frac{1}{\alpha \times ln(2\rho \Delta x^2 / c_0 h T_{PAT}^2 - 1/\alpha c_0)} \tag{3.15}$$

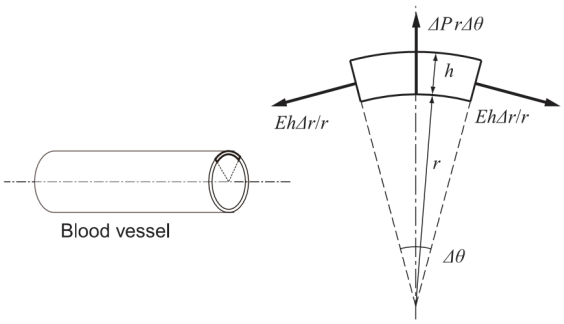

Figure 3.10.: Image of blood vessel's parameter: variation of the intravascular pressure Δp, variation of the blood vessels diameter Δr, the central angle of the blood vessel $\Delta\theta$ and E is the blood vessel's Young modulus of longitudinal elasticity. [22]

Equation 3.15 shows p_s the systolic BP in dependence of a constant concerning blood vessels characteristics α, blood density ρ, the distance between the pulse wave measure points Δx and the heart, the integration constant c_0 and the pulse arrival time $T_{PAT}(t)$.

Using the main principle of the relation between PTT and BP described in Equation 3.13 provides many different approaches for BP measurements. An interesting approach for the usage of the PTT is shown in Figure 3.11.

Pulse wave velocity method using Diode Laser

By recording the mechanical movements of the blood vessel's wall and using an ECG signal as reference signal, a time delay for different regions of the body is computed and additional information from the PPG signal can be used for evaluation. The blood vessel's profile is registered using a laser diode. This experimental device is able to detect the pulsation profiles of major arteries, including the profile of the pulse pressure. The laser light interacts with the human body and is backscattered by the skin into the laser. This leads to self mixing of the backscattered and generated laser light in the diode laser cavity, causing a change in the laser pump current. For registration of the changes two different methods are used: a photo diode or a resistor in series to the laser pump current. Figure 3.11 shows this experimental arrangement. Via an optical fiber the probing ray of the laser is guided to the skin surface. In this example Mp2 is placed

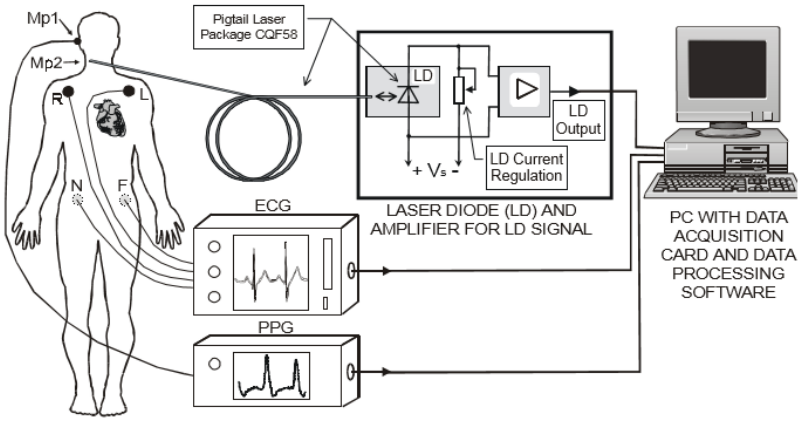

Figure 3.11.: Experimental arrangement for BP monitoring using the pulse wave delay; The mechanical movement of the vessels wall is registered by a laser diode. Via an optical fiber the probing ray is guided to the skins surface located at MP1 and MP2 and the time delay is calculated. As reference signal the ECG is recorded by a 4 leads system. Additionally, the PPG signal is measured and used for evaluation. [23]

close to the neck artery and MP1 is placed on the earlobe. As reference signal an ECG is recorded by a 4 leads system. Additionally, a PPG signal on the ear is measured. The developers were not able to measure the BP at this time because of very large dispersion in their measurements. [23]

3.4.3. Neural Network-based method using time domain features of the photoplethysmographic signal

This method is based on the PPG signal's shape and amplitude and the assumption that this shape correlates to the individual's blood pressure [24]. Figure 3.12 shows the parameters used for describing the PPGs signal shape. These time domain features are used for BP estimation. The 21 parameters chosen, include systolic time, the diastolic time and a ratio between them. Different times are extracted at 10 %, 25 %, 33 %, 66 % and 75 % the of PPGs amplitude. A feed-forward back propagation artificial neural network architecture with two hidden layers was used for the estimation. The MIMIC database was used for training and testing. Over

15000 cyles of different individuals were analyzed, the heart cycles of the different individuals were used in both train and test set. A resulting root mean squared error of 3.80 ± 3.36 mmHg for systolic and 2.21 ± 2.09 mmHg for diastolic pressure was achieved for the test set.[24]

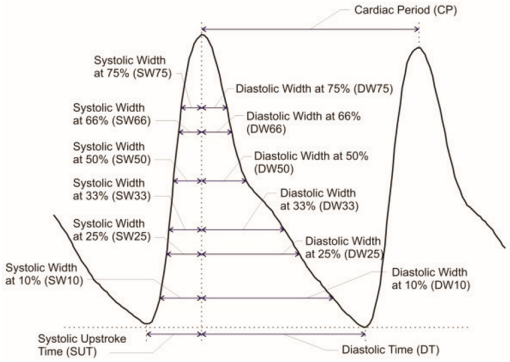

Figure 3.12.: The shape of the PPG signal, measured on the fingertip, is described by 21 parameters. This time domain features are fed into the neural network which is used for BP estimation [24].

3.4.4. Blood pressure estimation with FFT-based neural networks

This method described in [6] uses key features of the FFT of the PPG signal such as amplitudes and phases of cardiac components. As input for the FFT calculation one period of the PPG signal is extracted including 10 % of the previous and 15 % of the following heart cycle. On each extracted cycle an FFT is performed and the normalized amplitude and phase coefficients are use to train the neural network. In this paper data from the MIMIC II database are used as datasource including PPG measurements done at the fingertip and invasive continuous BP measurements. Because the used data is measured by commercial pulse oximeters, which had been highly amplified and filtered, the autor recommends this also for data from other sources. The single cycles were split into train and test set, cycles of the same individuals were present in both. As result for the test set, a fitting error of ± 7.08 mmHg for the systolic and ± 4.66 mmHg for the diastolic value was achieved. [6]

4. Solution

4.1. Data collection

4.1.1. Database data

Since measurements are very time consuming, for the first investigations database data was used. Several databases are provided by Physionet and can be downloaded at physionet.org.[8] The MIMIC database was selected for this propose. It provides physiological data which include invasive blood pressure measurements and synchronously measured PPG data on the fingertip. The PPG measurements provided on this database are highly filtered and preprocessed. 56 patients were used and up to 8 h of measurement per patient were downloaded. The provided data has a sampling rate of 125 Hz for both signals. For MATLAB and Python a toolbox called WFBD (WaveForm DataBase) is provided which can be easily integrated in those environments. To achieve a fast access to this data it was saved locally.

4.1.2. Sensor attributes, communication and User Interface

For own data collection, a proximity and ambient light sensor called PALS-2 from the Infineon Opto ASICS is used. This sensor integrates photodiodes and multiple LED driver outputs. The LEDs are driven in a pulsed operation mode, which makes the measurement and further the cancellation of ambient light possible. The proximity and the ambient light inputs are measured with 16 bit resolution, the maximum amount of driving current per LED is 200 mA and the maximum sampling rate is 250 Hz. The PALS-2 ASIC has two separate signal paths for proximity and ambient light functions. Three LED output pads are provided for

controlling external LED light sources in proximity mode. Figure 4.1 shows a block diagram of the PALS-2. [25]

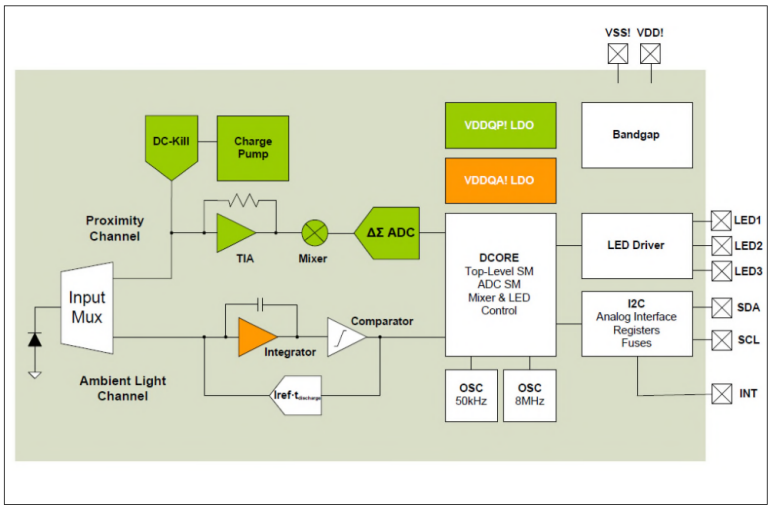

Figure 4.1.: PALS-2 block diagram

The used placement of the two LEDs and the photodetector is shown in Figure 4.2. The shown packaging was realized by OSRAM Opto Semiconductors. The PALS-2 photodetector is placed between two green LEDs, the components are fixed together in one housing.

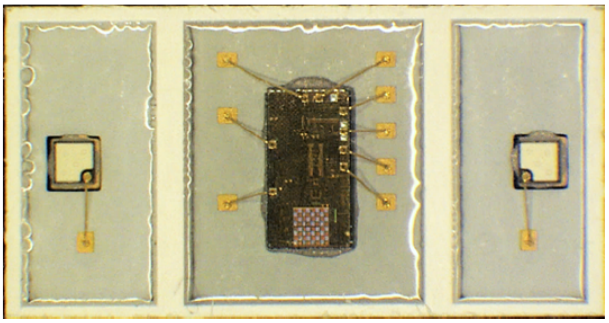

Figure 4.2.: Used packaging; Arrangement of LEDs and photodetector

The IFX PALS-2 demo board was used for data acquisition. This board contains the main components needed for communication with the PALS

as well as the power supply of the system and the PALS-2 device itself. In Figure 4.3 the demo board included in a wearable wrist watch fixture is shown. Figure A.1 in the Appendix shows the schematic of the used demo board.

Figure 4.3.: IFX PALS-2 demo board

For data monitoring and sensor communication a user interface was developed in Python. The data exchange between the program and the PALS-demo board is done via universal serial bus (USB) using the human interface device (HID) class. In the first steps the communication port is opened and the initialization of the sensors registers is done. At the initialization the oscillators of the sensor are trimmed and the sampling rate is set. To obtain similar data as provided on the database a sampling frequency of 128 Hz is used. New measured data is always placed on the opened port by the sensor. An interrupt occurs in case of new data and the data is fed into a queue were it waits for further processing. Another part of the routine is responsible for data preprocessing and displaying. The data is taken out of the buffer and stored internally. The preprocessing step as well as the update of the data displaying graph is triggered by a timer interrupt. To achieve a better performance only the last 10 seconds of data are used for live data processing (filtering etc.). The measured data can be stored in an .txt file for later usage. The user interface is shown in figure 4.4 To achieve an optimal utilization of the available measurement range a current regulation loop was developed. On a time triggered interrupt the system checks if the measured signal is within a certain ADC value range. If the amount of signal is too small, the LED driver current is increased.

In case of too high measured values, the possibility of clipping the PPG signal is high and the driver current is decreased.

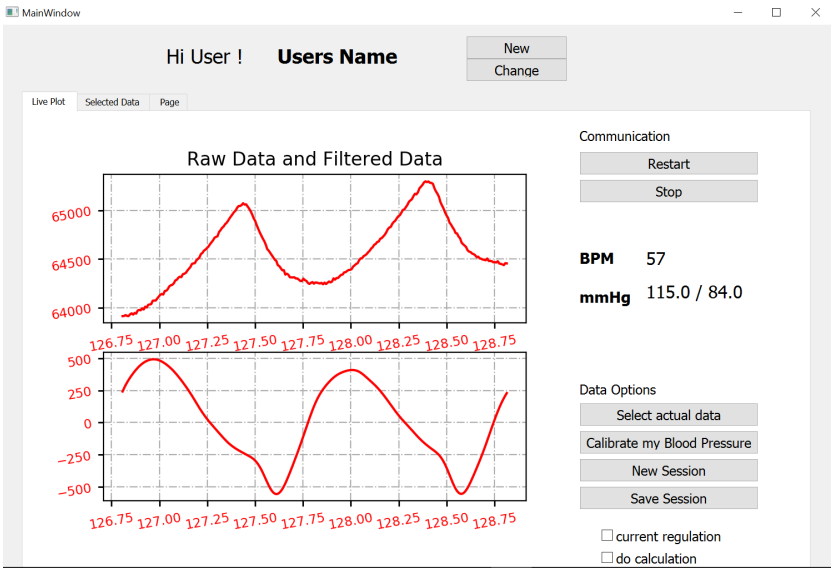

Figure 4.4.: User interface of the developed Python program; The upper signal represents the raw signal; the lower one the filtered, inverted signal.

4.1.3. Measurement setup

The continuous BP measurement was run using the Task Force Monitor simultaneously to the PPG measurement. The Task Force Monitor is a device using the Cardio vascular unloading technique described in Chapter 3.4.1 and measures the blood pressure continuously with a sampling frequency of 100 Hz. Figure 4.5 shows the used measurement setup. The arm cuff measures the absolute pressure which is used as calibration measurement. The finger cuff follows the continuous blood pressure.

The Task Force Monitor is very sensitive to the blood circulation of the test persons fingers. As explained in Chapter 3.4.1 the PPG signal is used to measure the change of the blood pressure over time. One of the observed limitations is that in case of to cold limbs the system was not able to detect the persons blood flow in the finger. A critical point of this setup is that the reference blood pressure is measured by an arm

Figure 4.5.: Measurement setup; Left arm: Task Force Monitor finger-cuff and PALS-2 demo board; Right arm: Task Force Monitor arm-cuff

cuff using the oscillometric method which is highly influenced by motion artifacts, positioning of the cuff and other factors like talking. The reference measurement itself is a challenge, and perhaps a more precise reference can be obtained by an invasive measurement.

4.2. Preprocessing

4.2.1. Band-pass filtering

Choosing proper filter coefficients represents a fundamental point in data processing. Disturbing effects should be filtered out; the shape which carries the information of the blood pressure should not be influenced. A digital IIR filter was used which filters the signal forwards and backwards to achieve a phase shift of 0 degrees (bidirectional filter). This is needed to prevent phase lags between the PPG and BP data after alignment which is discussed in Chapter 4.2.3. To achieve the best results, investigations

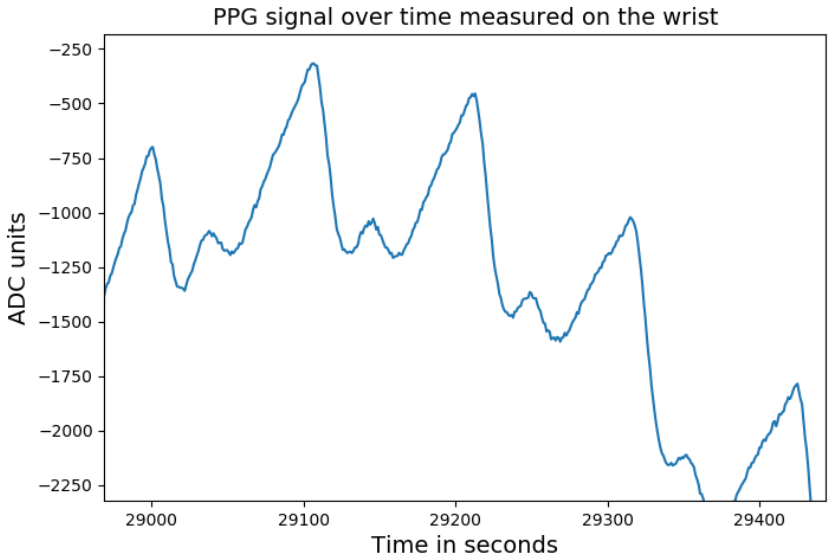

Figure 4.6.: Measured raw PPG data; Low frequency drift and high frequency noise; The signal was measured on the individuals wrist.

using different high-pass cut-off frequencies were made. Table 4.1 shows the achieved results for different cut-off frequencies. A predefined own measured dataset from one individual was used. The artificial network was trained for different cut-off frequencies, all other parameters of the whole system were kept constant. If the size of the dataset increases, also the time for the training process of the networks increases. Table 4.1 was the basis for further investigations using more train and test data.

This Table 4.1 shows that the results in the range of 0.5-0.7 Hz only differs in the range of 0.8 $mmHg^2$. Table 4.2 shows the achieved results in the predefined frequency range using train and test data of four different individuals (4000 heart cycles).

Theoretically, it is worse for the final result to filter too much information than to keep unnecessary frequencies. With correct usage of the neural network it should learn to ignore unneeded frequency components. On the other hand the low-pass filtering was necessary for the PPG heart cycle shape inspection. The high frequency noise should not disturb the comparison with the template as described later in Chapter 4.3. By using

Table 4.1.: Achieved results using data of one individual for adjusting the lower cut-off frequency; Settings of the artificial neural network: epochs max: 3000, batch size: 30: learning rate: 0.0002; Filter settings: filter order: 6, cut-off frequency low-pass: 9 Hz; The combined MSE for train and test data is shown for result assessment.

high-pass cut-off Hz	Train error $mmHg^2$	Test error $mmHg^2$
0.2	12.51	31.28
0.3	15.01	19.37
0.4	13.33	17.41
0.5	12.55	15.42
0.6	12.24	15.57
0.7	11.94	16.21
0.8	12.12	26.50

Table 4.2.: Achieved results using data of 4 different individuals for adjusting the lower cut-off frequency; Settings of the artificial neural network: epochs max: 7000, batch size: 300: learning rate: 0.0002; Filter settings: filter order: 6, cut-off frequency low-pass: 9 Hz; The combined MSE for train and test data is shown for result assessment.

high-pass cut-off Hz	Train error $mmHg^2$	Test error $mmHg^2$
0.5	45.44	51.35
0.6	43.35	48.29
0.7	39.10	45.77

to high cut-off frequencies for the low-pass the system was not able to match the PPG signal and the BP signal in the time domain using the correlation function as descried later in Chapter 4.2.3. By using the frequency spectrum of the PPG signal a cut-off frequency of 9 Hz was selected. The spectrum in Figure 4.7 shows that the amplitude components of the signal approach zero at approximately 9 Hz.

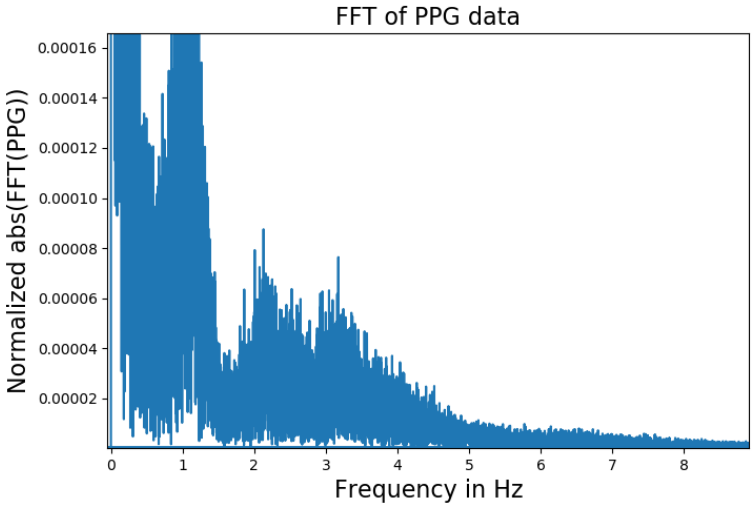

Figure 4.7.: Amplitude information of the PPG signal measured on the individuals wrist; Example of a amplitude spectrum showing the validity of the low-pass cut-off frequency decision. (unfiltered)

Table 4.3.: Order and cut-off frequencies of the applied IIR band-pass filter on the PPG signal

	Order	Cut-off frequency
Low-pass	6	9 Hz
High-pass	6	0.7 Hz

4.2.2. Data re-sampling

The sampling rate of the used systems for own data collection, as described in Chapter 4.1.3 is not equal for the PALS-2 and the Task Force Monitor. The sampling frequency of the Task Force Monitor measurement is about 100 Hz and the used frequency of the PALS-2 was set to 128 Hz. It is thus necessary to resample one of the signals to allow a direct comparison. The internal oscillators of the sensor were pre-trimmed using the I^2C interface via the HID class by programming the Low-Power Oscillator Trimming Register and the High-Performance Oscillator Trimming Register. Nevertheless, the effective sampling rate difference of the two different systems is not known and therefore the up- and down-sampling values have to be found. For this reason the FFT of the signals was calculated as shown in Figure 4.8.

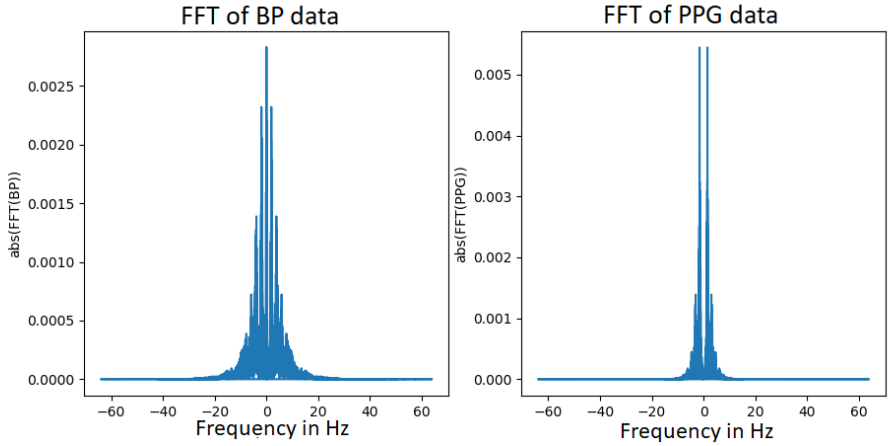

Figure 4.8.: Normalized magnitude of the FFT coefficients of the analyzed signals, the x-axis shows the frequency in Hz

In the left part of the Figure, showing the spectrum of the blood pressure signal, the main peak is shown at 0 Hz which represents the constant component. This main component is not available in the right spectrum because of the previous filtering of the PPG signal. The second dominant peak represents the carrier frequency of the physiological signal. This carrier is the beat rate of the heart and can also be found in the spectrum of the PPG curve. To obtain the same sampling rate for both signals,

the carrier frequencies have to be aligned. Figure 4.9 shows the carrier frequencies if a sampling frequency of 128 Hz is assumed for both signals.

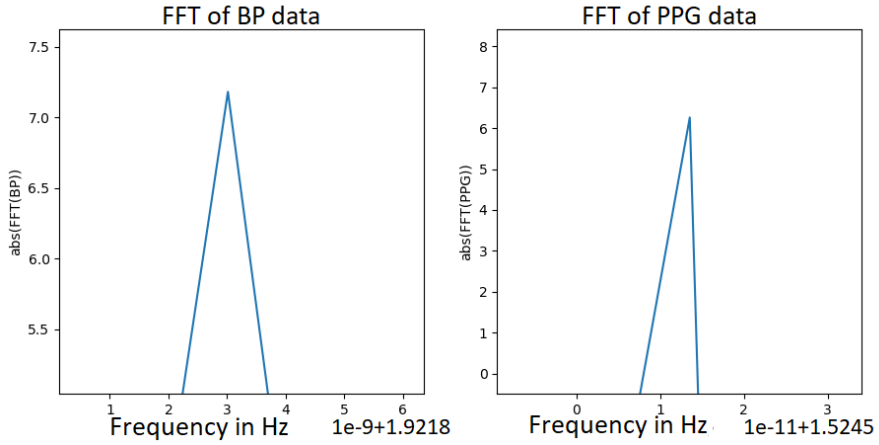

Figure 4.9.: Zoomed into carrier peak; Normalized magnitude of the FFT coefficients of the analyzed signals, the x-axis shows the frequency in Hz

It is taken as assumption that the carrier frequency of the PPG signal is correct and the carrier peak of the BP curve has to be adjusted. For both horizontal axes a sampling frequency of 128 Hz is chosen which is the sampling frequency of the PPG signal, and the frequency to be reached of the BP data. The peak on the right spectrum occurs at 1.52 Hz and on the left at 1.92 Hz. Since they are both coming from the same periodic process, the peak at the left spectrum has to be shifted to the right ones position. Equation 4.1 shows the expected proportion and Equation 4.2 the real occurring relation between the carrier frequencies. The used up an down sampling ratios can be found in Equation 4.3. By using the described method the accuracy of re-sampling depends on the the FFT resolution.

$$\frac{fs_{PPG}}{fs_{BP}} = \frac{128Hz}{100Hz} = 1.28 \tag{4.1}$$

$$\frac{fs_{PPG_{peak}}}{fs_{BP_{peak}}} = \frac{1.92Hz}{1.52Hz} = 1.26 \tag{4.2}$$

$$\frac{up}{down} = \frac{192Hz}{152Hz} = 1.26 \tag{4.3}$$

Due to the limited resolution of the FFT, a fine tuning of the phase adjustment is necessary. To find the remaining sampling difference, one heart cycle out of the PPG signal and the matching cycle of the BP signal were extracted. The length of both was calculated. The relation between the cycle durations was used for the final resampling of the BP signal. For up- and downsampling the Python function 'scipy.resample' was used. This function uses zero-padding in the frequency domain which corresponds to a sinc interpolation.

4.2.3. Data alignment

By using own measured data, it is necessary to align the signal measured by the PPG sensor and the Task Force Monitor. As data are collected on separate systems and as there is no possibility for triggering available, it is not possible to start the measurements at the same time. For phase alignment the correlation between the two input signals is calculated. The obtained information is used for shifting the curves. Because it is difficult for the human eye to confirm the correctness of the operation, this is done by looking at the heartbeat durations as shown in Figure 4.10. The heartbeat durations differ significantly from beat to beat and because of that it shows the time shift clearly. A small Python-script automatically aligns the two signals and crops overlapping data. It then stores the signals for further processing.

4.3. Quality assessment

4.3.1. Shape inspection

Physiological signals are very susceptible to artifacts and are typically varying a lot. There are various biological effects like variation in heart rate and cardiac output which lead to a change of the signal's width, height and morphology. The sensor's position can change, due to motion and a drift can overlie the useful signal due to different contact pressure. It is necessary to evaluate the quality of used signals. A method is required to automate the data selection for the ANN feature extraction. [26]

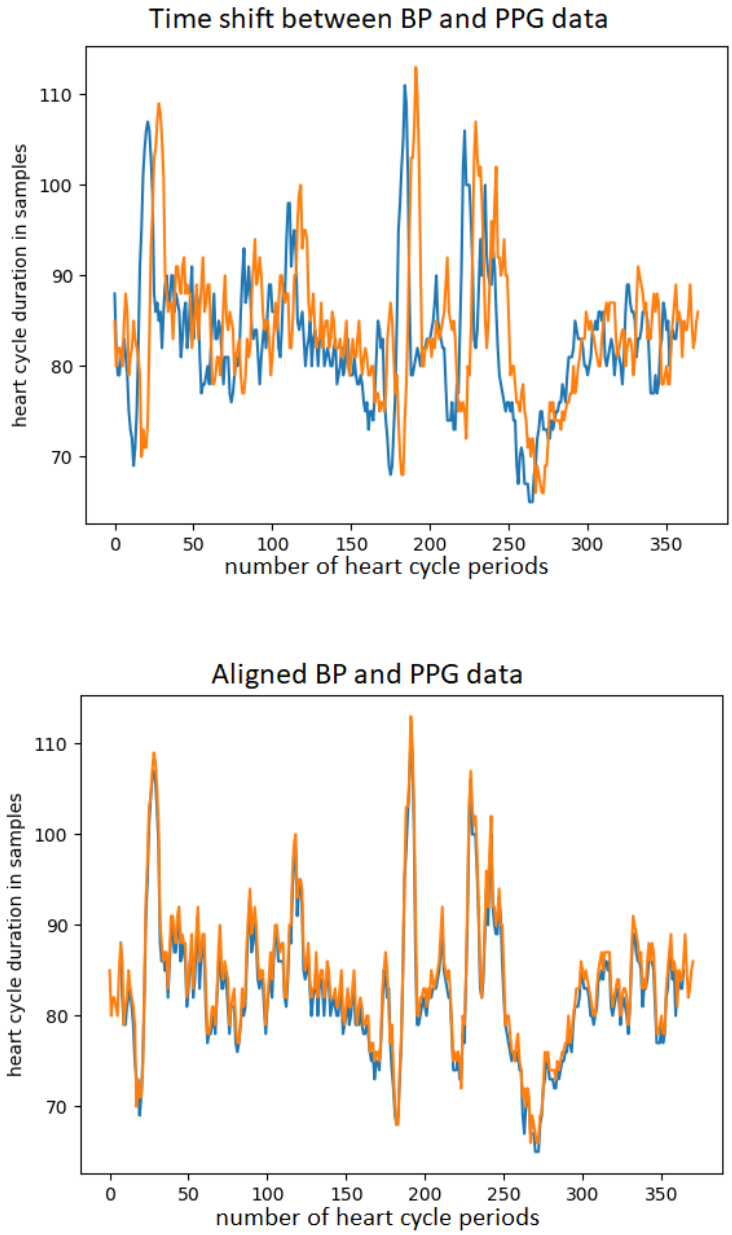

Figure 4.10.: Representation of the time-shift between the BP and PPG signals in the domain of heart cycle durations; Orange: heart cycle periods gained from PPG data; Blue: heart cycle periods gained from BP data Top: Not-aligned signals; Bottom: Heart cycle durations after correction of the phase lag

For quality assessment a procedure based on three steps has been developed as shown in Figure 4.11. At first a template out of all cycles

Figure 4.11.: Three steps of data quality assessment

is generated. In the second step this template is improved: every cycle is compared with the generated template and non-matching or less matching cycles are removed creating a new template with the remaining. In the last step every cycle is compared with the improved template and less fitting cycles are discarded from the available data. A flow chart breakdown for every step shows the quality assessment in detail. Figure 4.12 shows the initial template generation. The fist step represents the cardiac cycle extraction. A maximum and minimum detection is performed on the bandpass filtered input signal. The used algorithm detects only local minima/maxima which are at least 50 and a maximum of 150 samples apart and delivers the lowest minimum / highest maximum in this area. The signal is cut at every delivered minimum, the data between two minima represents one cardiac cycle. At first it is ensured that if there is a maximum between the two minima. In the next step every cycle is discarded with a non physiological length. The algorithm firstly selects cycles with a minimum length of 50 samples and a maximum length of 150 samples corresponding to 0.39-1.17 seconds. Cycles that do not fall into this range are discarded. The algorithm then normalizes all accepted cycles and computes a template by averaging them. The second step represents the generation of the improved template where an additional step compared to the initial template generation is inserted. For each cycle the similarity between the initial template and the actual cycle is calculated, in case of low similarity the cycle is discarded and not used in the improved template. The described procedure is shown in Figure 4.12 and 4.13. The third step is to check the similarity between the improved template and each cycle and is shown in Figure 4.14. Cycles with high similarity are used for further processing.

The similarity of the cycles is determined by calculating the covariance matrix of the template and the heart cycle to validate. The covariance matrix is a symmetrical matrix, in this case with the dimension 2x2. This means that the entry at position [1, 0] is equal to the entry at position [0, 1]. This values represent the diagonal data variance. The entries at position [0, 0] and [1, 1] are representing the parallel spread of the data. It was discovered, that the entry at position [0, 1], a measure of the positive parallel similarity between two vectors, differ most between good and faulty cycles. Thus, it was used as criteria to differ between those. Each heart cycle is normalized before the comparison using vector normalization.

The calculation of the covariance matrix was performed using the numpy.cov-funtion. The covariance compares two variables and indicates the level to which two variables vary together [27]. As described in the previous Section, the entry of the matrix at position [0, 1] was used to indicate the similarity. Figure 4.15 shows cut PPG cycles within a time period of < 30 seconds measured on the same individuals wrist. The sub-figure on top left shows all of these measured cycles, without shape-quality analysis. For further investigations two random good cycles and one bad cycle were selected and shown in the right top sub-figure. The left bottom of the Figure shows the selected good and bad cycles aligned on their maximum, zero-padded and normalized. In this condition their similarity was calculated as in the quality analysis procedure. Table 4.4 shows the calculated convolution values. The threshold for accepting or discarding the cycle has to be between the calculated values. Further covariances were calculated to determine what threshold would be acceptable. Flawed cycles should be rejected and the suitable ones should be kept. An value for this boarder is set to $1.5 \cdot 10^{-3}$.

Table 4.4.: Results of calculated covariance between good and bad cycles.

	Value of covariance
Good cycle 1 and bad cycle	$1.217 \cdot 10^{-3}$
Good cycle 1 and good cycle	$1.688 \cdot 10^{-3}$

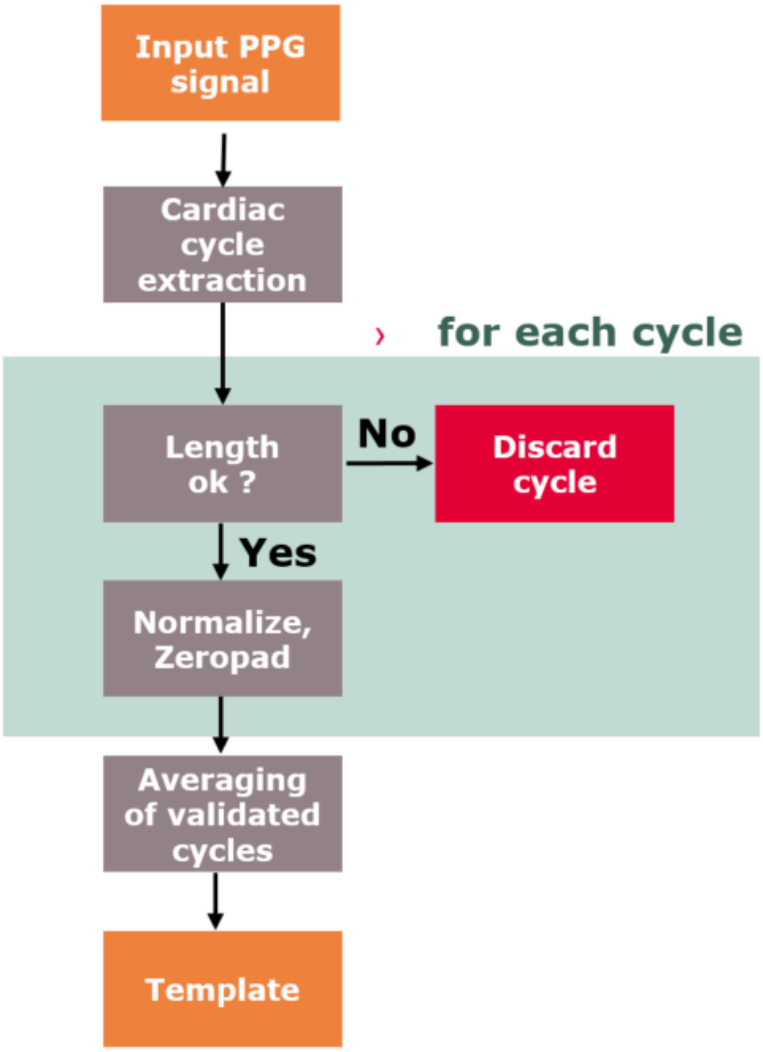

Figure 4.12.: First step of data quality assessment: The cardiac cycles are extracted from the measured PPG signal; Each normalized cycle with a non physiological length is discarded. The algorithm computes a template by averaging all accepted cycles.

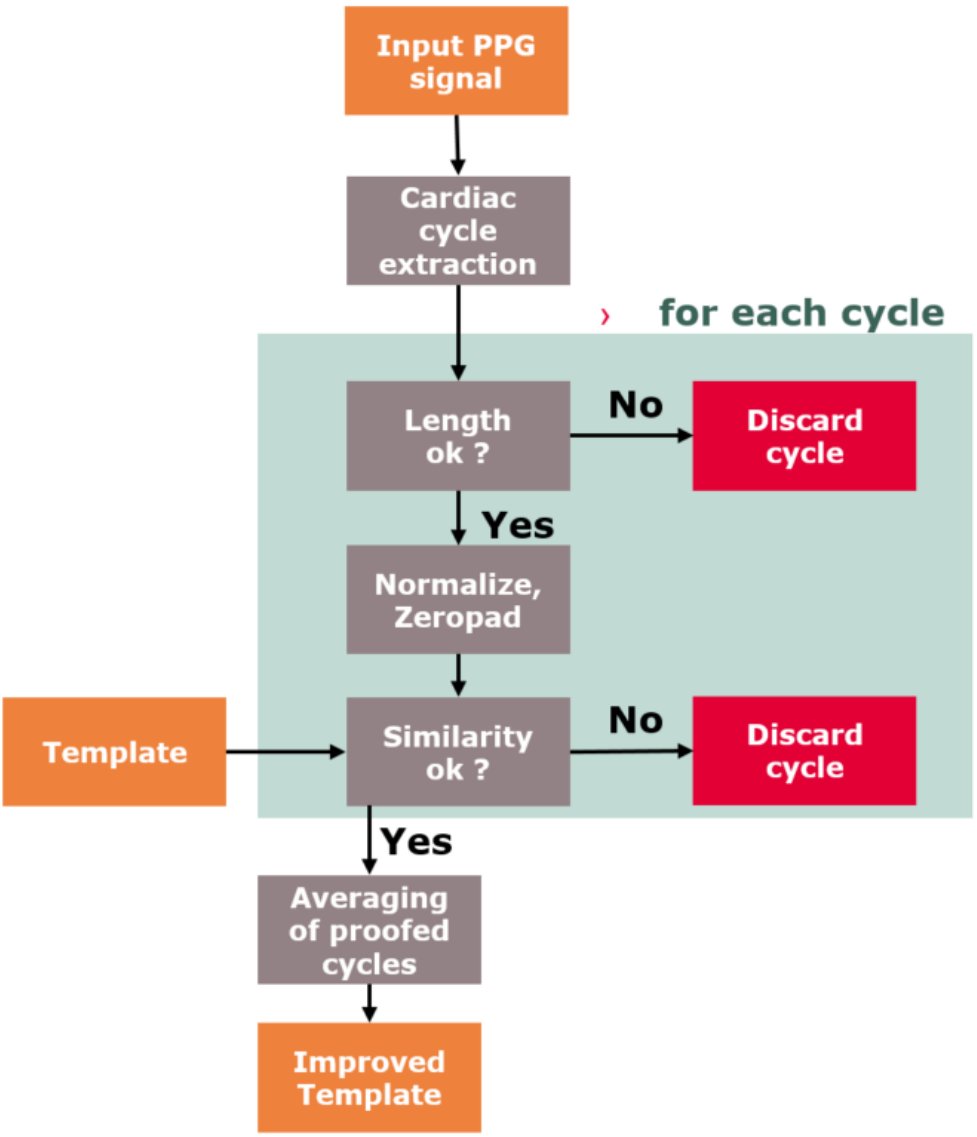

Figure 4.13.: Second step of data quality assessment: Cardiac cycles are extracted from the input PPG signal; Each cycle with a non physiological length is discarded. Each cycle is checked for similarity with the template, by calculating their covariance. Cycles with a similarity under a predefined limit are discarded. The algorithm then normalizes all accepted cycles and computes an improved template by averaging them.

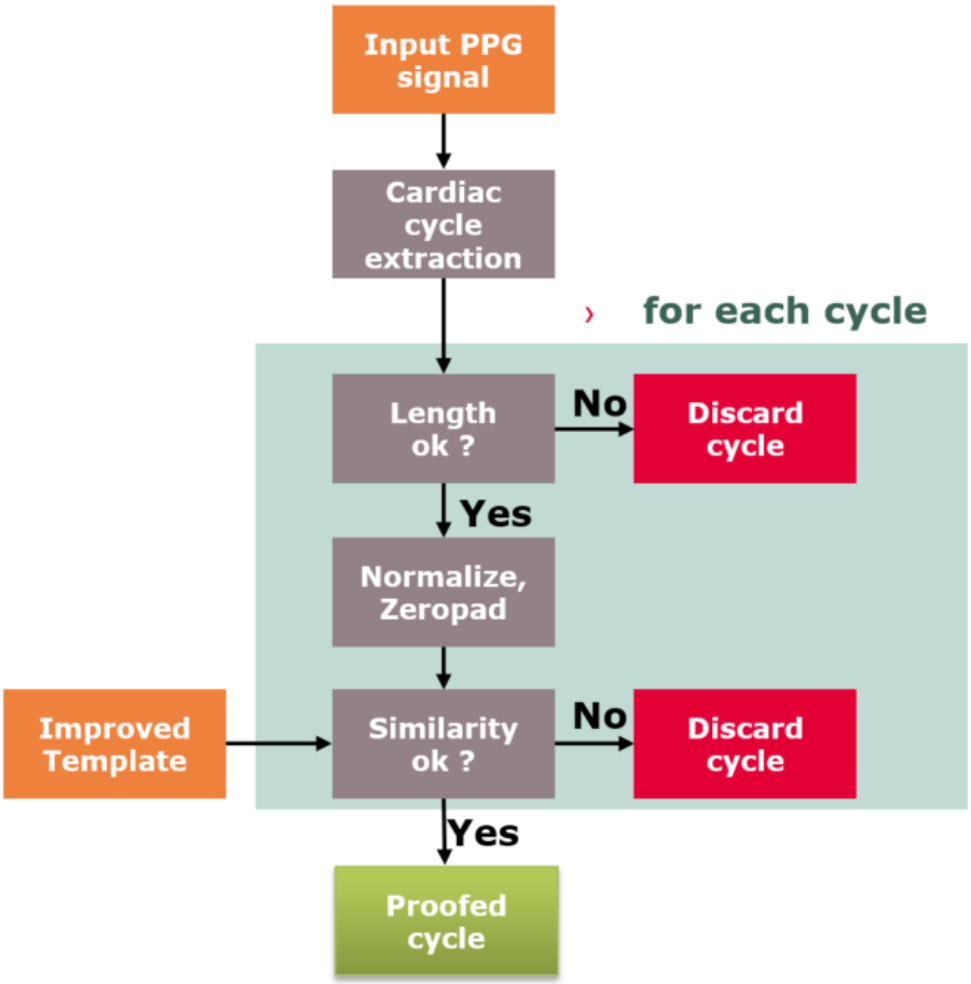

Figure 4.14.: Last step of data quality assessment: Cardiac cycles are extracted from the input PPG signal; Each cycle with a non physiological length is discarded. Each cycle is checked for similarity with the improved template, by calculation their covariance. Cycles with a similarity under a predefined limit are discarded.

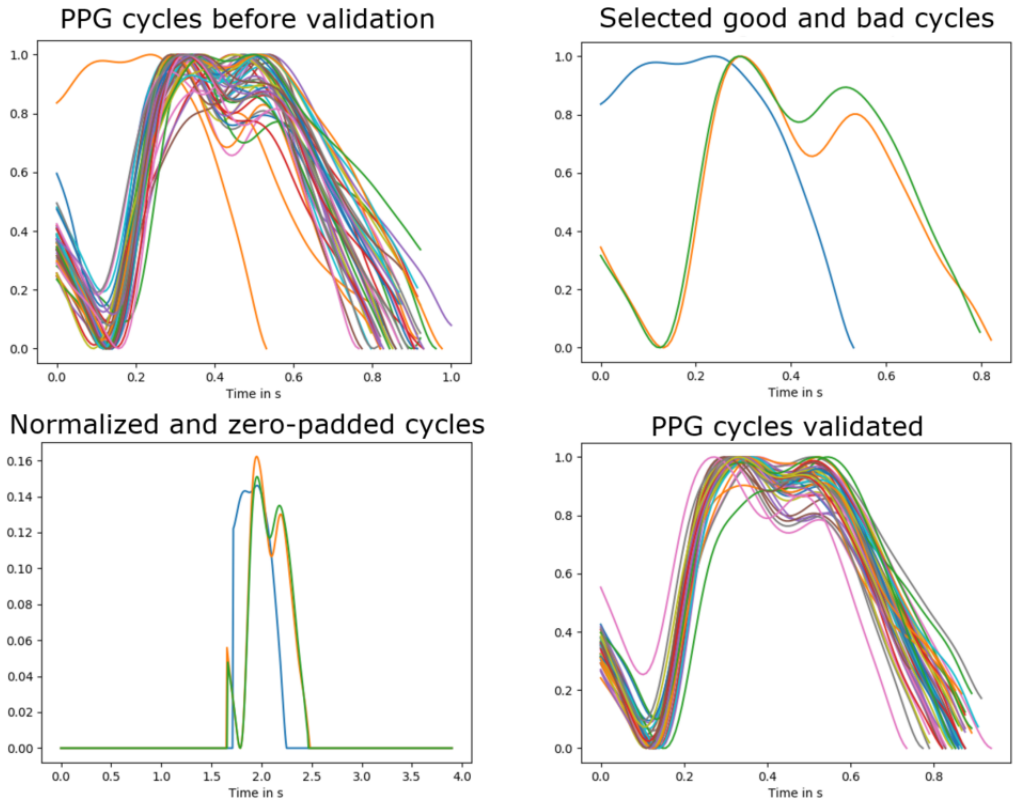

Figure 4.15.: Top left: Cut heart periods within 30 seconds of one individual. Top right: Selected bad and good cycles for further investigations, Bottom left: Selected cycles aligned on their maximum, zero-padded and normalized. Bottom right: Validated PPG cycles

4.3.2. Inspection of systolic and diastolic blood pressure values

To remove invalid non physiological blood pressure values which were not detected during the shape inspection, rules for plausible blood pressure values were applied. The rules are show in Table 4.5.

Table 4.5.: Applied rules for approved blood pressure values; Only heart cycles within this rule were used for further processing

	Systolic BP	Diastolic BP
	mmHg	mmHg
Minimum value	80	20
Maximum value	180	
Additional rule		syst - diast $>$ 20

4.3.3. Statistical distribution and data properties

As shown in Figure 4.16 the distribution of the used systolic and diastolic values can be approximated by a gaussian (normal) distribution. For later evaluation of the results it is necessary to consider the characteristic of the blood pressure data shown in Table 4.6 and 4.7. By the comparison of the deviation of the database data and own measured data it sticks out that the value of the standard deviation of the database data is almost twice as the standard deviation of the own measured data. This fact should be taken into account when assessing the achieved estimation.

To facilitate the learning process of the neural network, outliers of the train and test data are removed. In order to achieve good results the following rules are applied as shown in Table 4.8

Table 4.6.: Features of used database blood pressure data for training and testing the network

	Systolic	Diastolic
	mmHg	
Standard deviation	16.91	9.79
Mean	116.06	68.90

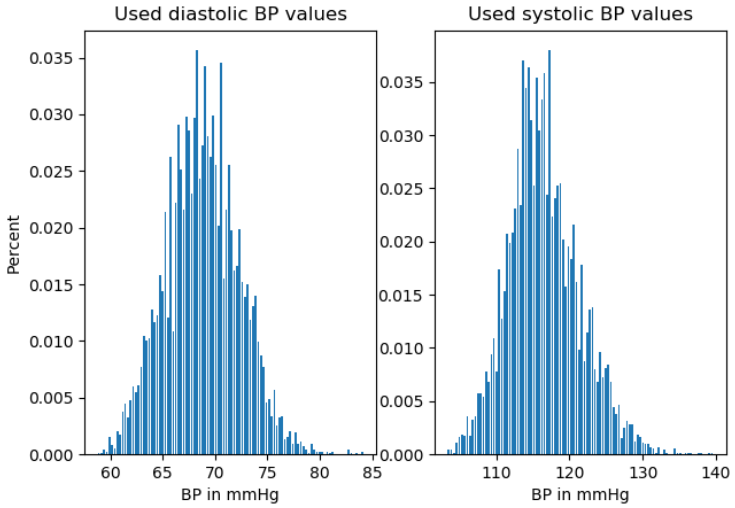

Figure 4.16.: Distribution of used database data (invasive measurement)

Table 4.7.: Features of own measured blood pressure data for training and testing the network; The reference pressure data was measured using the Task Force Monitor

	Systolic	Diastolic
	mmHg	
Standard deviation	10.55	8.05
Mean	119.24	85.73

Table 4.8.: Applied rules for statistical blood pressure control; Only heart cycles within this rule were used for further processing

Applied rules
1. systolic BP $\gtrless$ mean(systolic BP) $\pm$ 2 * std(systolic BP)
2. diastolic BP $\gtrless$ mean(diastolic BP) $\pm$ 2 * std(diastolic BP)

4.4. Feature extraction

A critical point of the work is the feature extraction out of the recorded preprocessed PPG signal. In literature different methods have been proposed. In this work the FFT coefficients of one heart pulse are used to train the ANN as suggested in [6]. In paper [6] is suggested that 10 % of the previous and 15 % of the following cycle should be extracted and used as input for the neuronal network. It is checked, whether these additional data points are actually needed using data of one individual as input of the ANN. The impact of different cycle length settings is shown in Table 4.9.

Table 4.9.: Achieved results using data of one individual for different data length; Settings of the artificial neural network: epochs max: 3500, batch size: 30, learning rate: 0.0004; The combined MSE for train and test data is shown for result assessment.

Previous cycle %	Following cycle %	Train error $mmHg^2$	Test error $mmHg^2$
10	15	2.64	2.91
10	0	3.21	3.42
0	15	3.311	3.32
0	0	2.93	4.1

All cycles have to be brought to the same length before the FFT calculation. This step was done by zero padding the extracted cycles in time domain. In frequency domain this step leads to constant frequency distances respectively to a constant frequency resolution of the FFT. Table 4.9 shows the impact of different heart cycle length. It seems that the impact of adding parts of the previous and following cycle is low; it should anyway be highlighted that the suggested 10 % previous and 15 % of the following

cycle lead to the best result. More FFT data points deliver more information for the neural network and deliver a slightly better result. It can be assumed that by using more than one heart cycle the error of the final result should be reduced. It should also be pointed out that the impact of using more successive cycles was not tested in this work and should be investigated in further projects. Along with investigations concerning the used signal input length, the choice of a suitable windowing before the FFT arises. Due to the long duration for calculations using the whole available dataset, data from one individual was used to investigate the impact of windowing. The used window function are shown in Figure 4.17. The result is shown in Table 4.10.

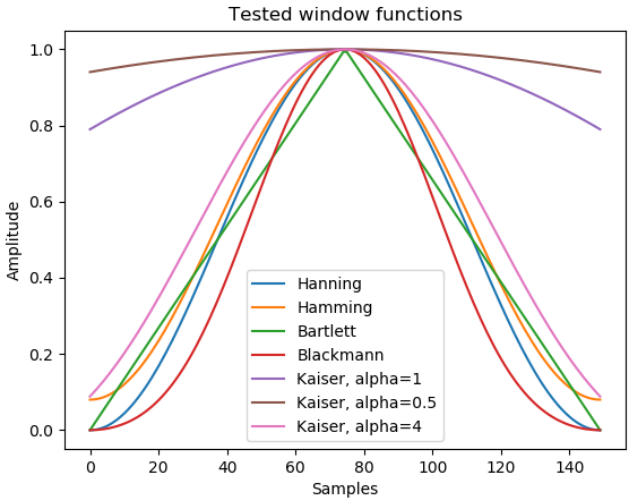

Figure 4.17.: Different applied window functions

As shown in Table 4.10 different window types have a different impact on the final result. The Hamming window leads to a better result with an error reduction of 0.8 $mmHg^2$ for the combined mean squared error compared to the non-windowed data. For the Kaiser window, different values for alpha were chosen and $\alpha = 0.5$ provided the best result. The impact of windowing by using data of the whole dataset is shown in the Chapter 5.1 results. After the calculation of the FFT of each extracted heart cycle, the amplitude coefficients were divided by the sum of all amplitude

coefficients to achieve a normalized representation. The DC part, which is represented at the 0 Hz frequency bin was not considered. Only one half of the spectrum was used as input for the neural network, since the other half is a mirrored replice for real input signals.

Table 4.10.: Achieved results using data of one individual for usage of different window functions; Settings of the artificial neuronal network: epochs max: 3500, batch size: 30, learning rate: 0.00025; The combined MSE for train and test data is shown for result assessment.

Window type	Train error $mmHg^2$	Test error $mmHg^2$
No window	3.33	3.65
Hamming	2.53	2.88
Hanning	3.59	3.74
Barlett	3.78	3.83
Blackmann	3.87	4.01
Kaiser, $\alpha = 0.3$	2.94	3.27
Kaiser, $\alpha = 0.5$	2.41	2.67
Kaiser, $\alpha = 0.7$	2.60	2.77
Kaiser, $\alpha = 1$	2.81	2.98
Kaiser, $\alpha = 4$	2.90	3.24

4.5. Artificial neural network

The neural network was developed using the Tensorflow library provided by Google in Python. A basic feed-forward structure with back-propagation was used. 300 input neurons including 150 for the phase and 150 for the amplitude features were used as input for the network for estimating the systolic and diastolic blood pressure value. This basic structure results from the idea that the calculation of the FFT coefficients of an 150 point curve results in 300 coefficients, 150 for the phase and 150 for the amplitude. By later optimization of the algorithm only the half sided FFT spectrum is fed into the neuronal network. This leads to an usage of only 150 input neurons and the network was optimized in further investigations.

Output calculation

In the network a standard matrix-vector multiplication is performed between the weights W and the layer inputs x. After the multiplication the bias vector b is added. This result is used as input for the Activation function. As activation function an hyperbolic tangent function is used.

$$y = tanh(W * x + b) \tag{4.4}$$

Network structure

Three hidden layers are used, it has been shown that more layers tend to over-fit the training data and do not lead to significant improvements. The first hidden layer has 150 input neurons and the second hidden layer 50 input neurons. The output layer is representing the systolic and diastolic BP and has two data points. The structure of the network is shown in Figure 4.18. After reducing the input layer of the artificial neuronal network to half, also the neurons of each hidden layer were halved.

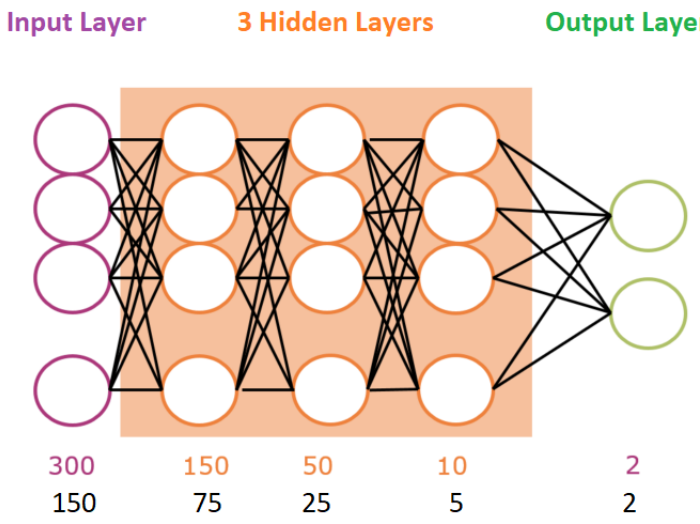

Figure 4.18.: Structure of the artificial neuronal network showing 300 input neurons, 3 hidden layers and 2 output neurons representing the diastolic and systolic blood pressure value. The updated network structure is represented by the lower neuron number.

For the training process a loss function has to be defined. The used loss

Table 4.11.: Achieved results on own measured data using different batch sizes; Settings of the artificial neuronal network: epochs max: 25000, learning rate: 0.00005; The combined MSE for train and test data is shown for result assessment.

batch size	Train error $mmHg^2$	Test error $mmHg^2$
350	62.45	68.12
300	47.93	64.47
250	59.12	64.23
200	52.49	65.05
150	48.98	71.01

function 'Mean Squared Error' tries to minimize the sum of the mean squared errors of the systolic and diastolic values between the estimated values and the desired results. The weights are initialized with random values with a standard deviation of 0.0001. The optimal batch size was figured out by training the whole network using different batch sizes.

As shown in Table 4.11 batch sizes between 300 and 200 are ideal for the training of the neural network. The smaller the learning rate the less the weights are adjusted per trainings step and the more steps are needed to find a local minimum which in this case is met more precisely. Nevertheless, due to the limited time available, the used learning rates are in the range of 0.0005 and 0.00005. For fast investigations higher learning rates are used, for achieving final results, smaller learning rates are used. Due to the random initialization of the network weights each training process is individual and not reproducible. To prevent from landing in a bad local minimum, it is necessary to carry out the training process several times. The epoch is a measure for the amount of performed training steps. In case of a too small epochs the trained network is under-fitted, in the opposite case over-fitting occurs. The realization of the final networks can be found in the following Section 5. If the network is trained once the used structure, weights and biases are stored and can be reused for estimating current blood pressure values from the photoplethysmographic signal.

4.6. Feature extraction using wavelets

Additionally to the FFT features, the possibility to describe the heart cycles shape using the Wavelet transformation was investigated. It should be noted that the whole system is set on the FFT features and just some fast experiments were made to discover the possibilities of Wavelets. All described steps were done as for the frequency features. Only the feature extraction step on the preprocessed and selected cycles was adapted. Due to the limited time expansion of the Wavelets it seems plausible that they can describe the heart cycles shape more precisely. By cutting out one single heart beat of the PPG signal, mathematically a multiplication with the rectangular window is performed. This multiplication leads in the frequency domain of the FFT to a convolution with a sinc function. This convolution strongly affects the coefficients. This step is changed by the usage of the Wavelet transformation. It is a special technique which describes a general function through a sum of a Wavelet series. The basic idea is that a signal can be decomposed out of a particular set of functions obtained by dilating and shifting one single function. This specific wave is called the mother-Wavelet. The key feature of the Wavelet analysis is the time-frequency localization. In contrast to the Fourier transformation, the energy of the Wavelet is restricted to a finite time interval. [28]

Figure 4.19 shows the Daubechies mother-Wavelet.

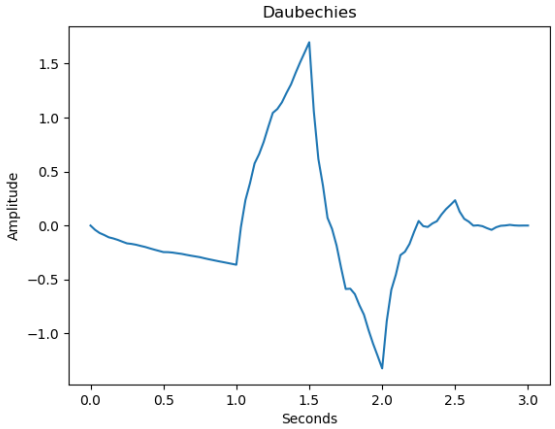

Figure 4.19.: Waveform of Daubechies mother-Wavelet

By applying the wavelet transformation, two different types of coefficients are calculated. The first coefficient is representing the scaling and the second the time shift of the mother-Wavelet. The continuous wavelet transformation of a function f(t) at a scale α and position τ is given by the following equation. [29]

$$Wf(\alpha,\tau) = \frac{1}{\sqrt{\alpha}} \int_{-\infty}^{+\infty} f(t)\Psi^{+}(\frac{t-\tau}{\alpha})dt \tag{4.5}$$

Where Ψ^{+} denotes the complex conjugation of the mother-Wavelet. Equation 4.5 means that the signal to be analyzed $f(t)$ is convolved with stretched and dilated copies of the mother wavelet. For $\alpha < 1$ the wavelet is contracted and the transformation delivers information about finer details of $f(t)$. In case of $\alpha > 1$ the mother wavelet is expanded and the transformation delivers a coarse view. [29]

The discrete wavelet transformation analyses the signal at different frequency bands, with different resolution. The signal is decomposed into a coarse approximation and detailed information. This step is related to high- and low-pass filtering. The mother wavelet is in this case interpreted as the filters impulse response. The basic procedure is shown in Figure 4.20. Each stage consists of two digital filters and two down sampling stages by a factor of 2. The first filtering step is described by the mother wavelet (high-pass) and its mirror-version (low-pass) (magnitude response mirrored at $\pi/2$). The down sampled outputs after the first high- and low-pass provide detail information D1 and its approximation A1. A1 is then further processed. The wavelet transformation acts like a mathematical microscope. It is zooming in like a microscope into small scales and it is zooming out in case of large scales. [28]

The achieved number of coefficients depends on the input signal length. The Python command 'pywt.pwt' delivers 150 coefficients from a signal length of 150 samples. This means that 75 coefficients describing the approximation and 75 coefficients describing the details are delivered. [28] shows that the Daubechies Wavelet leads to the best result for electroencephalography (EEG) signal classification. Because of that proposal this mother wavelet was used for superficial investigations. After performing the transformation the calculated coefficients were fed into the neural network as described in Chapter 4.5.

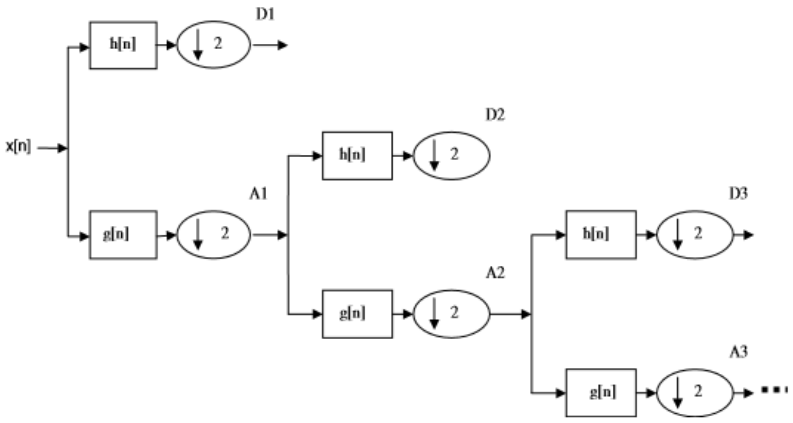

Figure 4.20.: Sub-band decomposition using Wavelets; $h[n]$ represents the high-pass, $g[n]$ the low-pass filter. [28]

4.7. Summary of the used parameters

As mentioned in the previous chapters, two different data sources were used for training and testing of the neural network. The optical PPG signal was measured on the fingertip in case of the database data and on the wrist in case of own measured data. After signal preprocessing, 10 % of the previous and 15 % of the following cycle in addition to the actual cycle, were extracted out of the signal. After the quality assessment of each cardiac period and the adjustment of the length, the FFT or the Wavelet transformation was performed. The dataset containing different individuals was shuffled and spit into train and test data. The test data was used for training the network, in other words used for weight adjustment. The resulting weights are applied on the features of the test data to estimate their blood pressure values. The used parameters for filtering, quality assessment and feature extraction for own measured data and database data are summarized in Table 4.12. The same parameters are used for FFT as well as for the Wavelet feature extraction. Only the parameter of the used neural network were adjusted as shown in Table 4.13.

Table 4.12.: Finally used parameters for filtering, quality assessment and feature extraction.

Parameter type	Parameter	Value	
Filtering	Order low-pass	6	
	Order high-pass	6	
	Cutt-off frequency low-pass	9	Hz
	Cutt-off frequency high-pass	0.7	Hz
Quality assessment	Convolution value for accepted cycle	0.0015	
Feature extraction	Attached previous cycle	10	%
	Attached following cycle	15	%
Window	Rectangular window		
	Kaiser window	$\alpha = 0.5$	

Table 4.13.: Finally used parameters for the artificial neuronal network for different data sources and different feature extraction.

Feature	Data	Epochs	Batch size	Learning rate
FFT	Database	9000	200	0.0001
FFT	Own measured	7500	200	0.0001
Wavelet	Database	700	200	0.005

4.8. Definition of the used errors

4.8.1. Root mean squared error

The root mean squared error ($RMSE$) is the standard deviation of the prediction errors called residuals. They measure how far from the regression line data points are; and how spread they are [30]. It is used in prediction analysis to verify experimental results.

$$RMSE = \sqrt{\frac{1}{N}\sum_{i=1}^{N}(z_{f_i} - z_{\sigma_i})^2} \tag{4.6}$$

where z_{f_i} are the expected values, z_{σ_i} are the observed values and N is the number of values [30].

4.8.2. Mean squared error

The mean squared error indicates how close a regression line is to a set of data points. In this thesis the artificial neural network is using the sum of the squared error of the systolic and diastolic values. The advantage of using the mean squared error for the training process is, that it gives more weight to larger differences [30].

$$MSE = \frac{1}{N}\sum_{i=1}^{N}(z_{f_i} - z_{\sigma_i})^2 \tag{4.7}$$

4.8.3. Mean bias error

The mean is the average of a data set [30]. The mean bias error (MBE) shows the average of the prediction error; the bias of the regression line.

$$MBE = \frac{1}{N}\sum_{i=1}^{N}(z_{f_i} - z_{\sigma_i}) \tag{4.8}$$

4.8.4. Standard error

The standard error(std(E)) in this thesis describes the standard deviation of the errors.

$$std(E) = \sqrt{\frac{1}{N}\sum_{i=1}^{N}((z_{f_i} - z_{\sigma_i}) - MBE)^2} \tag{4.9}$$

5. Results

5.1. Results on database data

The resulting estimated pressures achieved by the usage of FFT feature extraction are compared to the invasive measured pressure data. As a measure of the error the root mean squared error (RMSE), the mean bias error and the standard deviation of the error are used. The achieved result on database train data (500.000 heart cycles) and test data (150.000 heart cycles) of 56 different individuals is shown in Table 5.1. To get a better insight into the achieved accuracy of the estimated BP values compared to the invasive measured pressures, histograms for the diastolic and systolic errors are constructed to show the error distribution in Figure 5.1.

	Train data		Test data	
	Systolic	Diastolic	Systolic	Diastolic
	mmHg		mmHg	
Standard error	8.06	4.29	9.24	4.71
Mean bias error	0.02	0.09	0.01	0.08
Root mean square error	8.06	4.29	6.18	3.25

Table 5.1.: Achieved results on test data using the same trained network for blood pressure estimation for all individuals from the MIMIC database; The errors are representing the difference of the estimated values compared to the invasive measured data

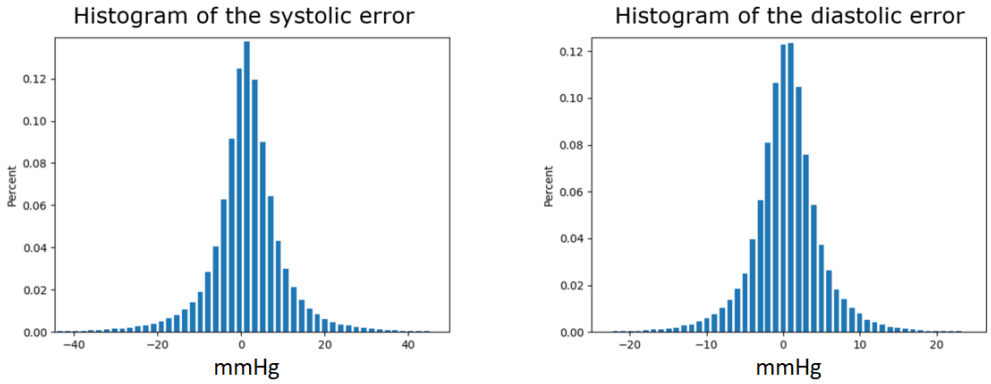

Figure 5.1.: Histogram of the estimated systolic and diastolic BP values compared to the invasive measured pressure; The error deviation of the test data from the MIMIC database is shown. (Kurtosis systolic:13.31 diastolic: 7.41)

Figure 5.2 shows the measured and estimated blood pressure values of the database test data in mmHg. The shown test data was not used for training and represents mixed heart cycles of all 56 individuals in a random order.

Figure 5.3 shows the achieved result on not-mixed database test data. This means that successively measured pressure values of individuals are shown in actual chronological order. Measurements of different persons were lined up. To show the trend of the pressure and better visualize if the estimated values can follow this drift, an average of the estimated and measured pressure values over ten heart cycles was made.

Table 5.2 shows the achieved results with additional usage of windowing. A comparison with Table 5.1 shows that the performance of the kaiser window is worse compared to the rectangular window.

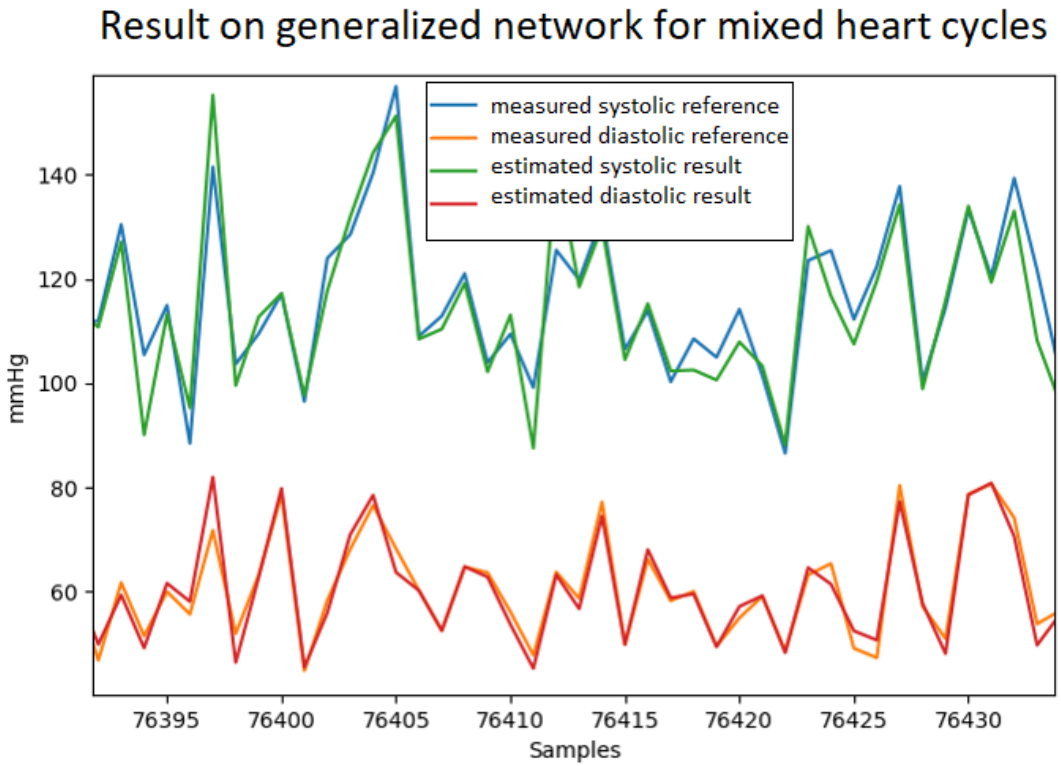

Figure 5.2.: Estimated and invasively measured systolic and diastolic blood pressure values of the testing data in mmHg; Final result for database data by using over 500.000 heart cycles from 56 different test persons for training and 150.000 cycles for testing; Shuffled heart periods from all test persons in a random order (Zoom)

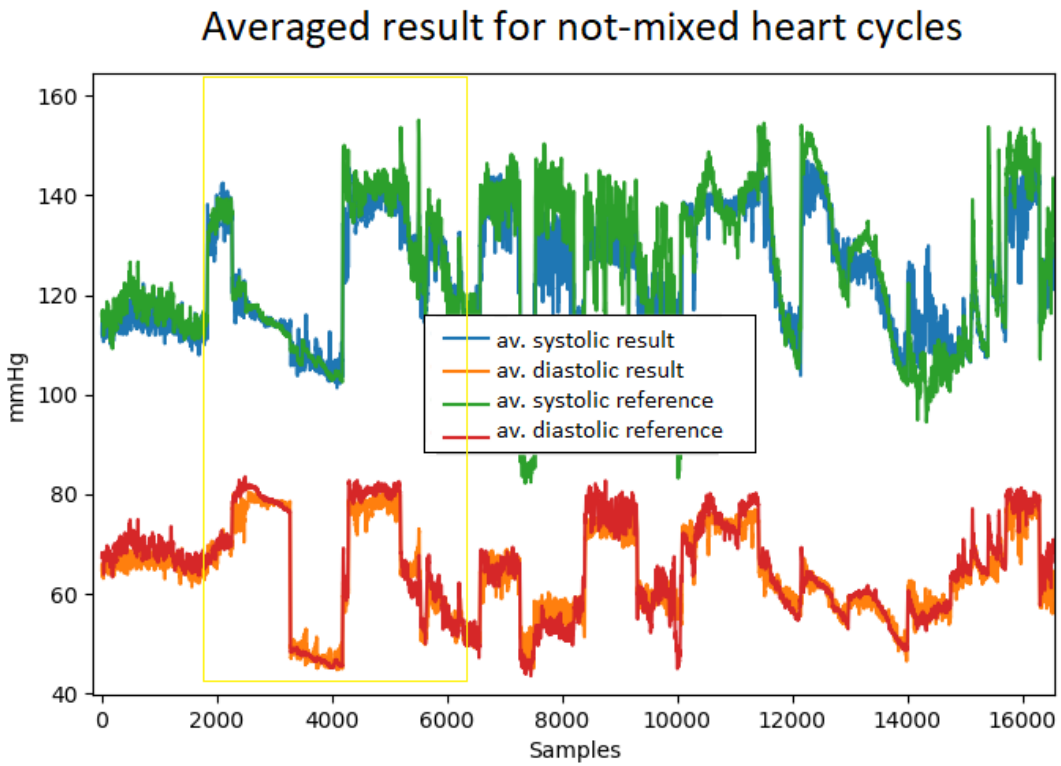

Figure 5.3.: Estimated and invasive measured systolic and diastolic blood pressure values of the testing data in mmHg; Final result for database data by using over 500.000 heart cycles from 56 test persons for training and 150000 cycles for testing; Averaged heart periods over 10 cycles in chronological order; For averaging a moving average filter was applied, the resulting edges were cut off; Measurements of different persons were lined up

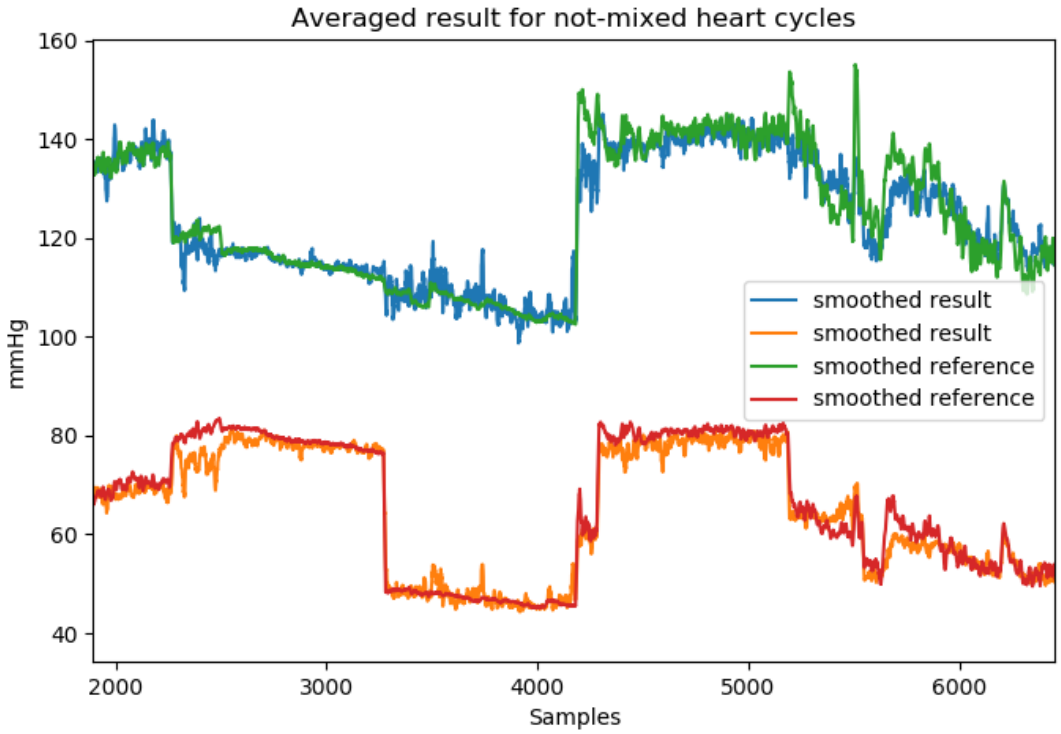

Figure 5.4.: Estimated and invasive measured systolic and diastolic blood pressure values of the testing data in mmHg; Final result for database data by using over 500.000 heart cycles from 56 test persons for training and 150000 cycles for testing; Averaged heart periods over 10 cycles in chronological order; For averaging a moving average filter was applied, the resulting edges were cut off; Measurements of different persons were lined up (Zoom 5.3)

Kaiser window α = 0.5	Train data		Test data	
	Systolic	Diastolic	Systolic	Diastolic
	mmHg		mmHg	
Standard error	8.72	5.09	9.99	5.39
Mean bias error	−0.23	−0.06	−0.27	−0.06
Root mean square error	8.72	5.09	10.00	5.39

Table 5.2.: Achieved results on test data from the database for blood pressure estimation for all 56 individuals; The errors are representing the difference of the estimated values compared to the invasive measured data; Windowing was performed on the PPG cycles used for training and testing before the calculation of the FFT coefficients.

Up to now the network was trained and tested with different heart cycles of all available individuals. To examine the possibility of estimating blood pressure from the PPG signal also for individuals not included in the training set, an additional network was trained. For this purpose 5 random people were excluded from the trainings set and the data of the remaining 51 individuals was used to train the neural network. The achieved results for individuals whose heart cycles were not included in the trainings set are presented in Table 5.3 and shown in Figure 5.5. In the Figure the heart cycles of of these 5 individuals are lined up and the persons are numbered. The Figure shows that the estimation achieves different accuracy for different individuals. In particular, for test person 2 the mean bias error is significantly increased, even if the trend seems to be still followed in the estimation.

	Test data	
	Systolic	Diastolic
	mmHg	
Test person 1		
Standard error	14.53	4.13
Mean bias error	5.34	−12.81
Root mean square error	15.49	13.45
Test person 2		
Standard error	11.32	5.07
Mean bias error	−30.53	−8.98
Root mean square error	32.56	10.30
Test person 3		
Standard error	27.32	11.43
Mean bias error	2.01	3.12
Root mean square error	27.39	11.84
Test person 4		
Standard error	15.94	8.13
Mean bias error	−4.37	−2.34
Root mean square error	16.53	8.46
Test person 5		
Standard error	5.41	4.09
Mean bias error	−1.95	−2.25
Root mean square error	5.75	4.67

Table 5.3.: Achieved results on database test data for the 5 persons not included in the training set; The errors are representing the difference of the estimated values compared to the invasive measured data

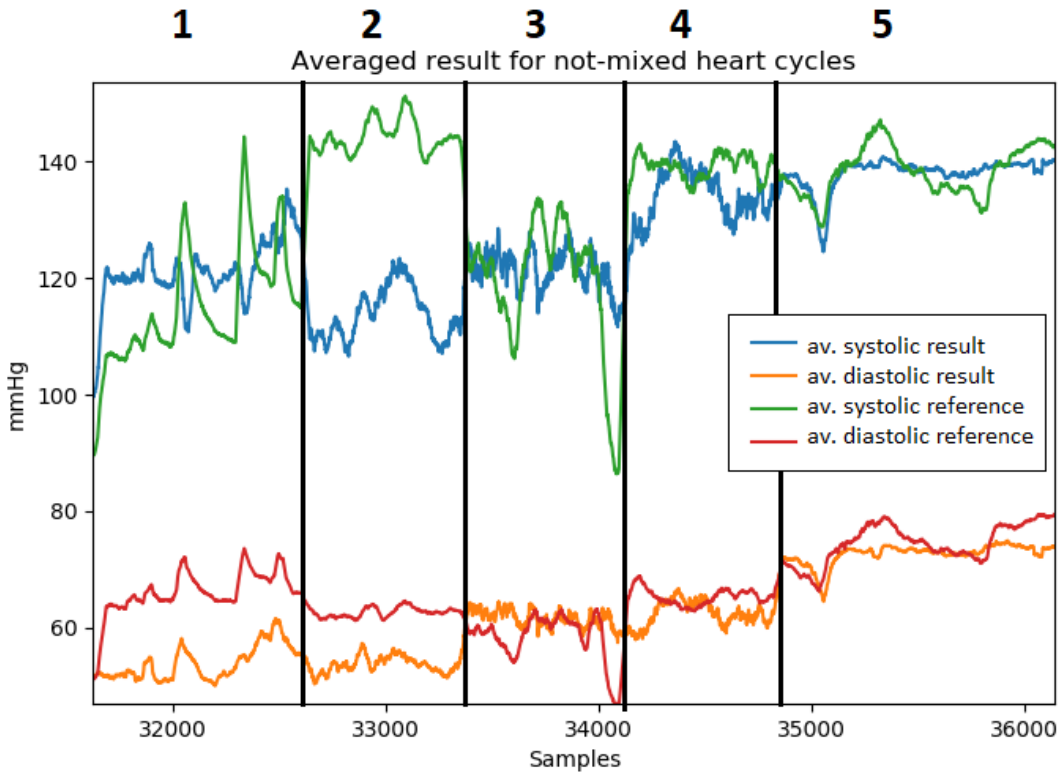

Figure 5.5.: Estimated and invasive measured systolic and diastolic blood pressure values of the testing data in mmHg; Heart beats of individuals witch were not included in the training set; Averaged heart periods over 10 cycles in chronological order; For averaging a moving average filter was applied, the resulting edges were cut off; Measurements of different persons were lined up

5.2. Results on own measured data

The neural network was trained and tested using data from 16 different individuals with average measurement time of 15 minutes per person. The continuous blood pressure reference measurement was done using the Task Force Monitor. The photoplethysmographic signal was measured on the wrist using the PALS-2 sensor. Over 6000 heart cycles were used to train the generalized network and 2000 were used for testing. Table 5.4 shows the final result for investigations based on own measured data. Histograms of the error of the systolic and diastolic estimated pressure values compared to the Task Force Monitor measurement are shown in Figure 5.6.

	Train data		Test data	
	Systolic	Diastolic	Systolic	Diastolic
	mmHg		mmHg	
Standard error	6.22	4.72	7.83	5.93
Mean bias error	−0.23	−0.11	−0.33	−0.22
Root mean square error	6.22	4.72	5.79	4.34

Table 5.4.: Achieved results for estimation on own measured data; The data was collected using the Infineon Opto Asics PALS-2 on the wrist

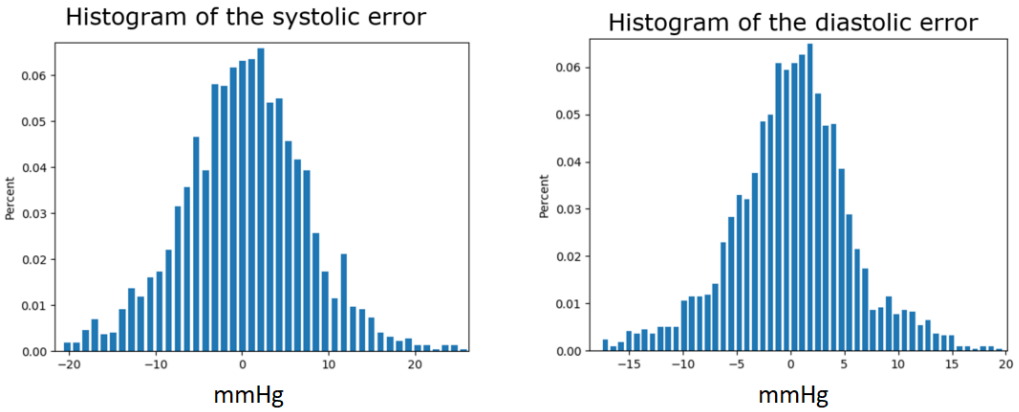

Figure 5.6.: Histogram of the errors of the test data for estimated systolic and diastolic BP values; The reference measurement was done using the Task Force Monitor (Kurtosis systolic:4.98 diastolic: 3.38)

Figure 5.7 shows the values of the reference measurement and estimated blood pressure of own measured test data in mmHg. The heart cycles of the testing set are shown in a random order. The estimated and measured results of non-mixed data for different patients are shown in Figure 5.8. This Figure should visualize that the estimation error varies for different individuals. Some are underestimated and others are overestimated. A moving average filter over 10 periods was applied for smoothing the BP data results. It can be seen that some sections (individuals) are better described by the model than others.

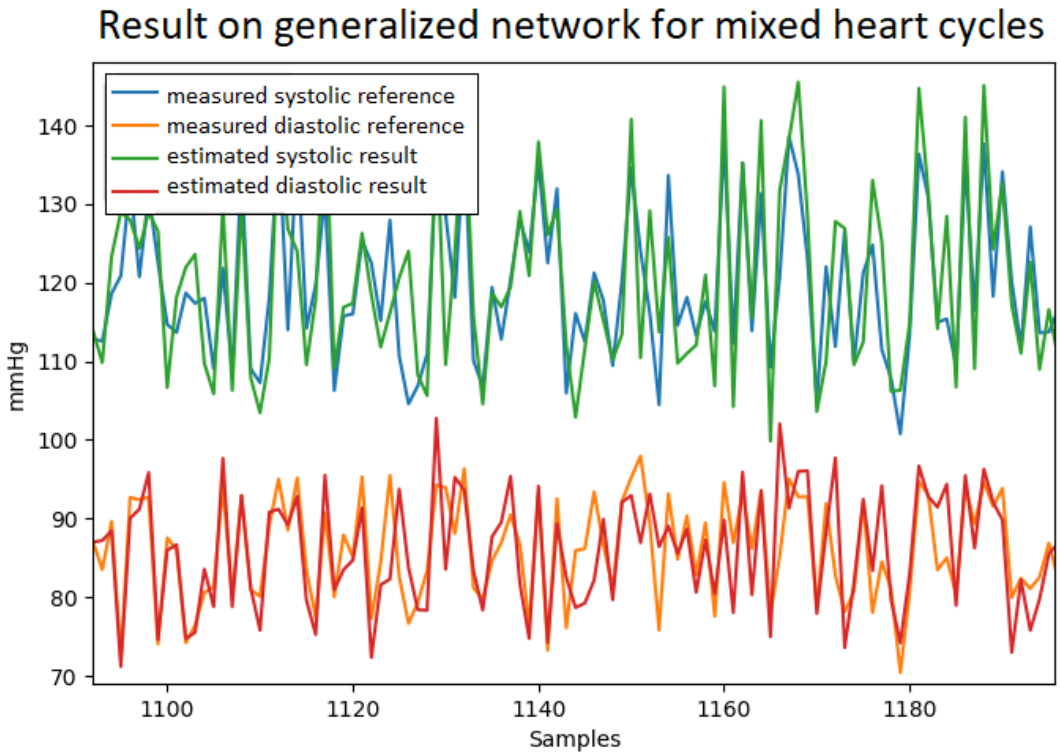

Figure 5.7.: Estimated measured systolic and diastolic blood pressure values and reference measurement of the testing data in mmHg; Final result for own measured data using the PALS-2 on the wrist; Shuffled heart periods from 16 individuals in a random order (Zoom)

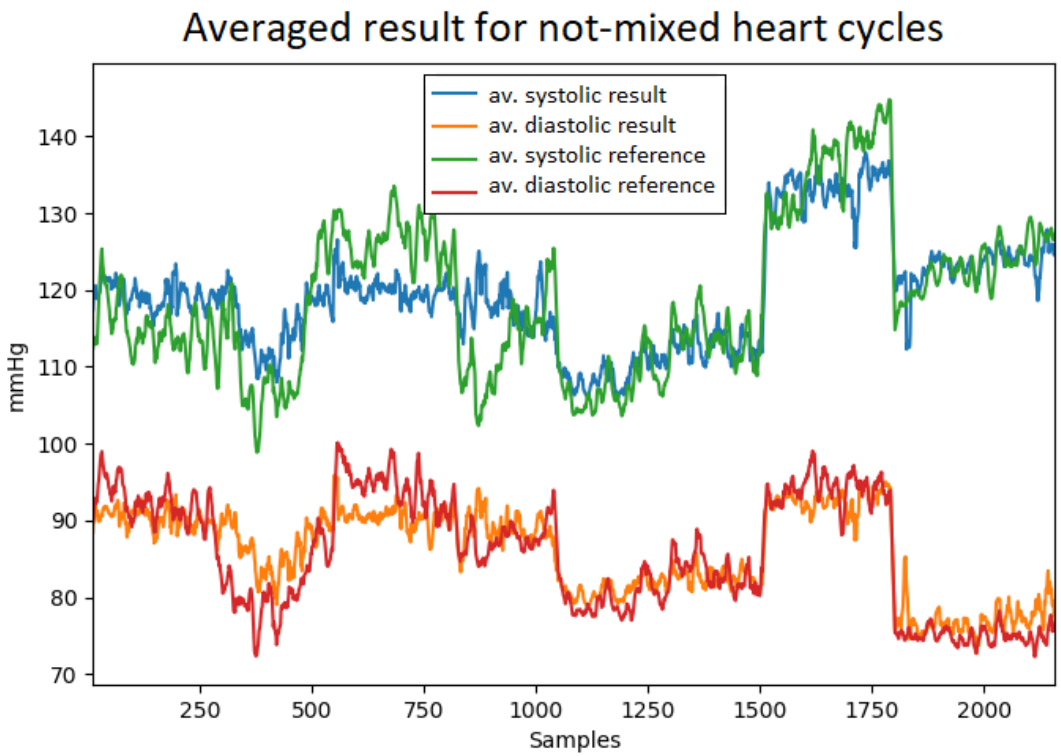

Figure 5.8.: Estimated result and Task Force measurement for systolic and diastolic blood pressure values of the testing data in mmHg; Final result for own measured data using the PALS-2 on the wrist; Heart periods of 16 individuals lined up in chronological order; Estimated and measured pressure values are averaged over 10 heart periods. For averaging a moving average filter was applied, the resulting edges were cut off (Zoom)

To investigate the possibility to estimate blood pressure also for individuals not included in the training set, three more individuals were measured. The weights and biases, which were calculated earlier, were applied on the PPG features to estimate the blood pressure. Table 5.5 shows the achieved results for those persons, whose heart cycles are not included in the training set. Figure 5.9 shows the averaged result over 10 cycles for not-mixed heart cycles for different individuals. The first section shows estimated and measured blood pressure values of persons whose cycles are not included in the training set. The right section shows the measured and estimated values of heart cycles of persons included in the training set. It is worth noting that different cycles of those individuals were used for training compared to those used for testing. Before the training process started the extracted cycles were split into a train and test set.

	Test data	
	Systolic	Diastolic
	mmHg	
Test person 1		
Standard error	6.25	5.75
Mean bias error	6.24	−5.07
Root mean square error	8.83	7.66
Test person 2		
Standard error	11.72	10.60
Mean bias error	5.75	−0.67
Root mean square error	13.052	10.63
Test person 3		
Standard error	9.42	8.18
Mean bias error	0.69	−1.42
Root mean square error	9.45	8.31

Table 5.5.: Achieved results on own measured test data for the 3 persons not included in the training set; The errors are representing the difference of the estimated values compared to the data measured with the Task Force Monitor.

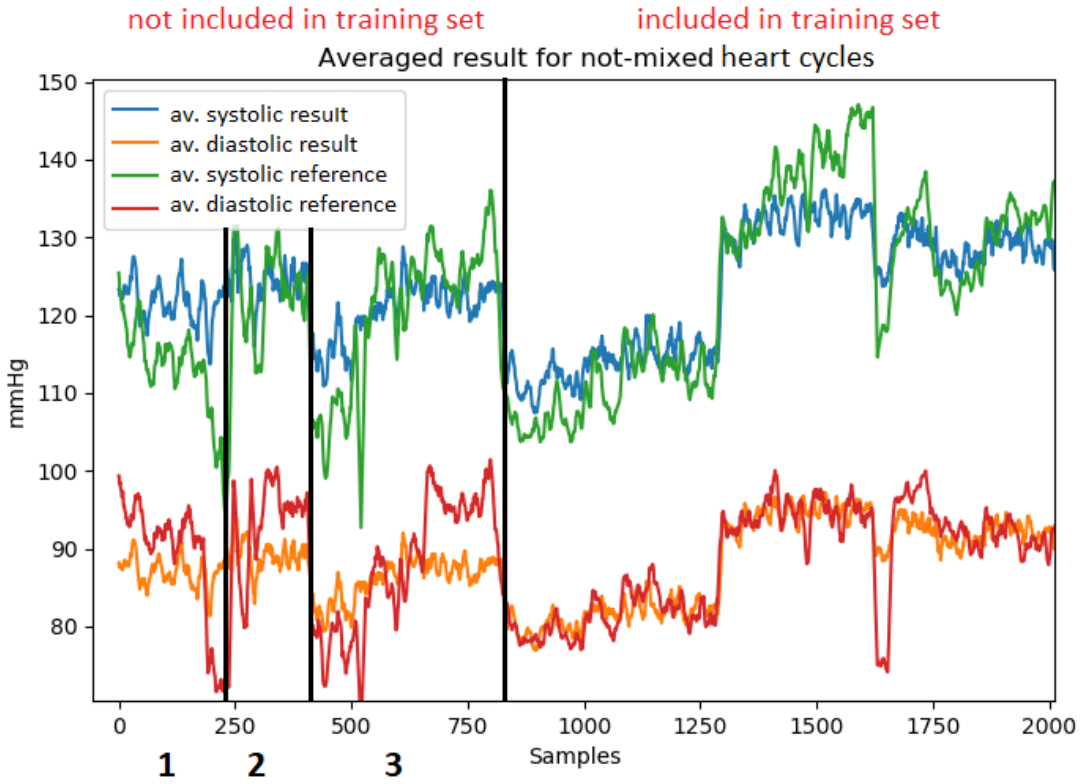

Figure 5.9.: Estimated pressure for individuals included and not included in training set; Left section: estimated and measured pressure values for heart cycles from individuals not included in the training set; Right section: Estimated and measured pressure values from individuals whose other measured cycles are used for training; Own measurement using the PALS-2 sensor for PPG signal acquisition and the Task Force Monitor for the reference measurement.

5.3. Results using the wavelet transformation

This section gives a short outlook about the possibility to estimate BP from the optical measured signals using the wavelet transformation. As mother Wavelet the Daubechies Wavelet was used. Database data of all 56 individuals provided from the MIMIC database were used for training and testing. As described in the previous chapters the heart-cycles were split into a train and test set. The parameters of the ANN were adjusted. All other parameters of the system were not modified compared to those used for extracting the FFT features. In comparison with the achieved parameters of the FFT features, in particular the results for the systolic values were improved. The achieved results are shown in Table 5.6 and the distribution of the systolic and diastolic error is shown in Figure 5.10. How accurate the estimated pressure can follow the invasive measured pressure is shown in Figure 5.11 and Figure 5.12.

	Train data		Test data	
	Systolic	Diastolic	Systolic	Diastolic
	mmHg		mmHg	
Standard error	7.60	4.28	7.08	4.49
Mean bias error	−0.08	−0.31	−0.26	−0.87
Root mean square error	7.60	4.30	4.98	3.15

Table 5.6.: Achieved results on test data using the same trained network for blood pressure estimation for all 56 individuals; The errors are representing the difference of the estimated values compared to the invasive measured data

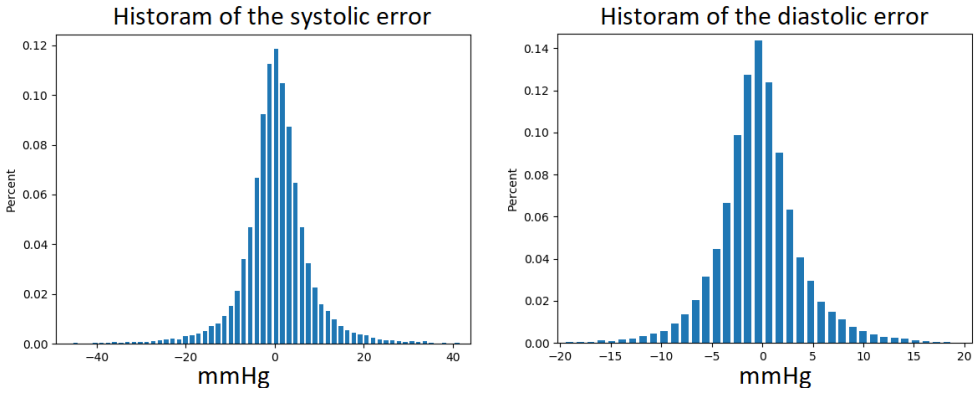

Figure 5.10.: Histogram of the errors of the test data for estimated systolic and diastolic BP values; The reference measurement was done using the Task Force Monitor; For the feature extraction the Wavelet transformation was used.

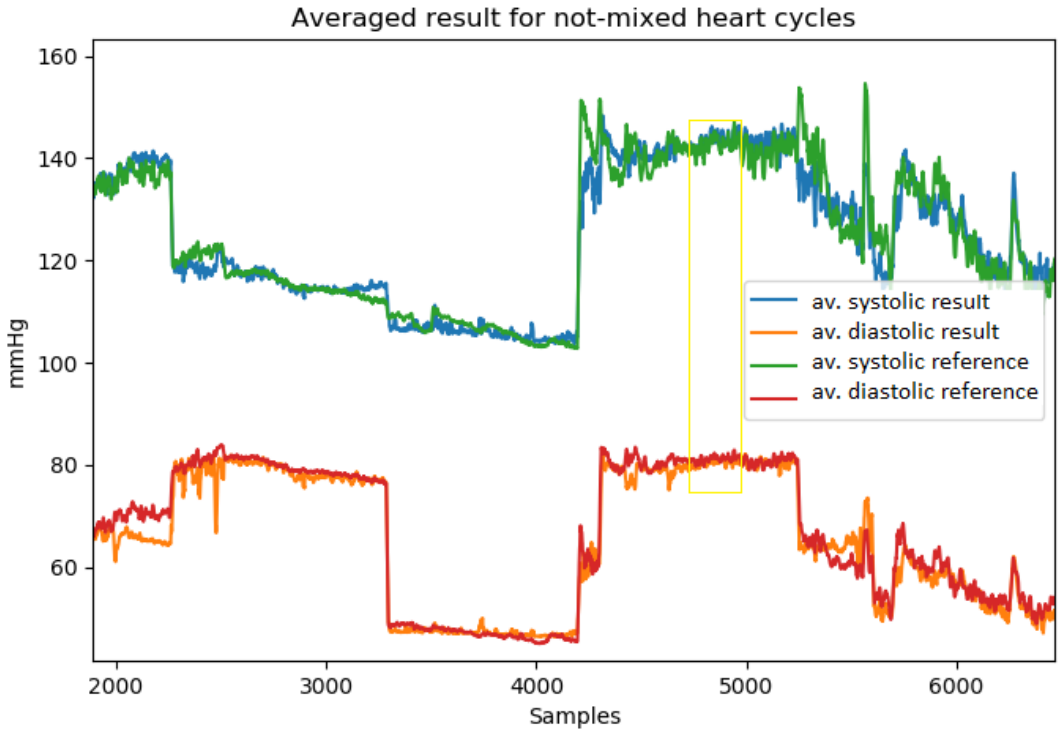

Figure 5.11.: Estimated and invasive measured systolic and diastolic blood pressure values of the testing data in mmHg; Final result for database data by the Wavelet transformation; Not-shuffled heart periods from 56 individuals are lined up. Remaining average of 10 samples; For averaging a moving average filter was applied, the resulting edges were cut off. (Zoom)

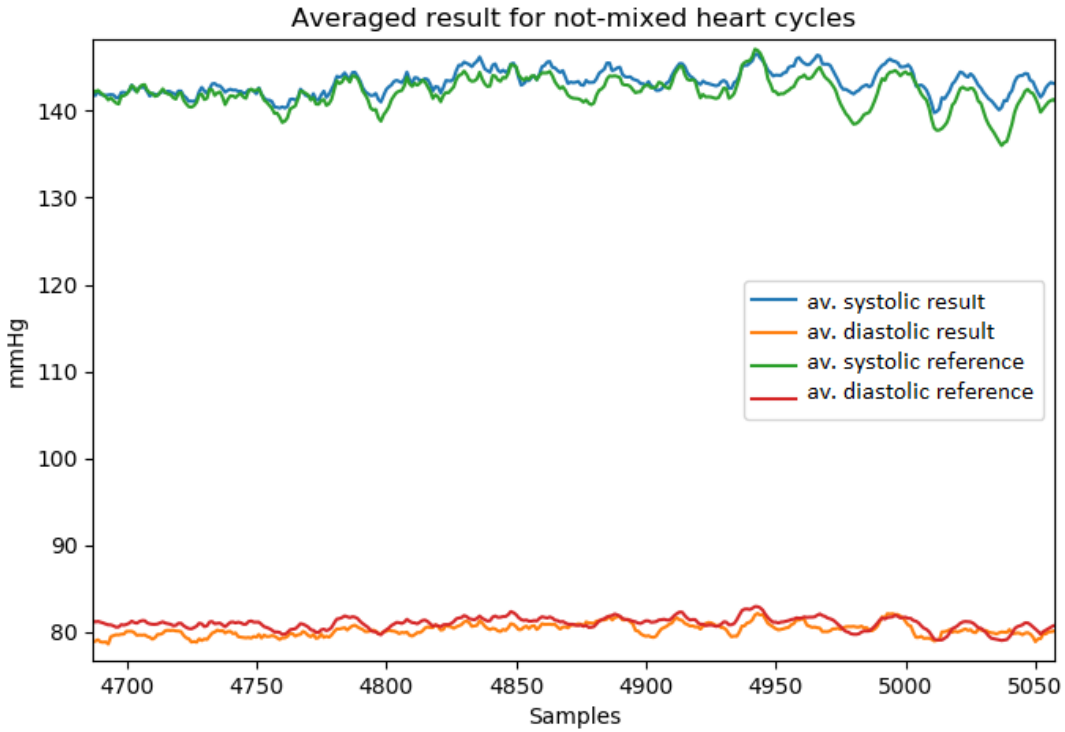

Figure 5.12.: Estimated and invasive measured systolic and diastolic blood pressure values of the testing data in mmHg; Final result for database data by the Wavelet transformation; Not-shuffled heart periods from 56 individuals are lined up. Remaining average of 10 samples; For averaging a moving average filter was applied, the resulting edges were cut off. (Zoom of Figure 5.11)

5.4. Examination on trained weights

This chapter deals with the drive to understand the correlation between blood pressure and PPG signal. For this reason the trained network achieved with the FFT features was analyzed. The following figures visualize the trained weights and biases. In general, it is very difficult to interpret the coefficients of a neural network. It has to be noted that the input layer is multiplied with the weights; the multiplied input layer and the biases are summed; afterwards the activation function is applied ($y = tanh(W * x + b)$) as descried in Chapter 4.5. A neural network is basically an advanced fitting process. Each training procedure is individual due to random weight initialization and normally no result is identical to the others. The target is to find a global minimum for the error, but in general only a local minimum can be found. This section shows the trained weights for the database data; due to the larger dataset it is assumed that they are describing a wider population. To visualize the weights of the input layer a 3 dimensional plot is used. The x-direction represents the neurons of the input layer (75 representing the FFT amplitude and 75 representing its phase), the y-direction the input to the first hidden layer and the z-direction the weights value. The frequency resolution of the FFT is given with Equation 5.1.

$$\Delta f = \frac{f_s}{N} \tag{5.1}$$

with f_s the sampling frequency, Δf the frequency resolution and N the number of samples. The calculated frequency resolution for our setup is therefore given with Equation 5.2.

$$\Delta f = \frac{128Hz}{150} = 0.853Hz \tag{5.2}$$

Figure 5.13 shows the first hidden layer for the reduced network with 150 input neurons. The weights of the input neurons representing the phase information are weighted low compared to the weights of the amplitude information. In general it looks like that the weights representing amplitude information in the range of 4-8 Hz, represented by the input neurons 5-10, are having the highest values.

Further layers and biases are more difficult to interpret. The weights and biases of all layers are summarized in Figure 5.13 and 5.14. On the y-axis the neuron input of the specific layer are shown, on the x-axis the neurons representing the output.

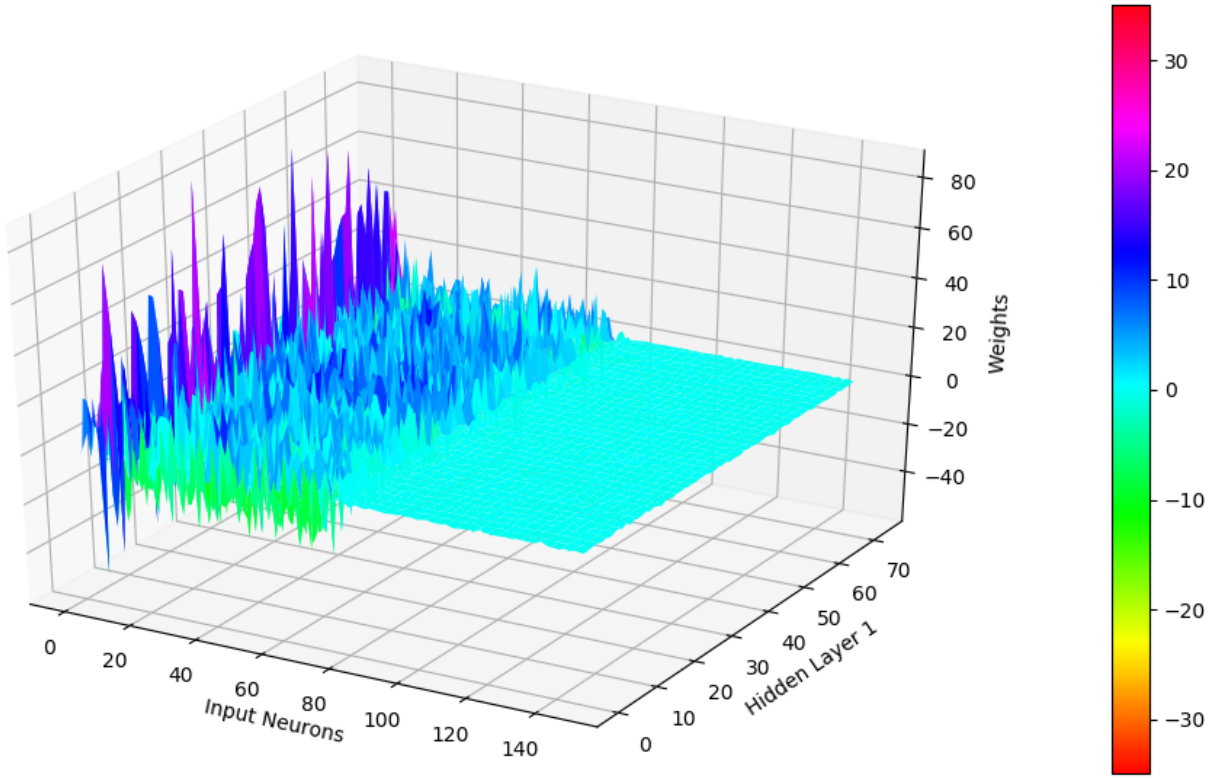

Figure 5.13.: 3D representation of the weights between input layer and first hidden layer; Achieved on database data by usage of the FFT

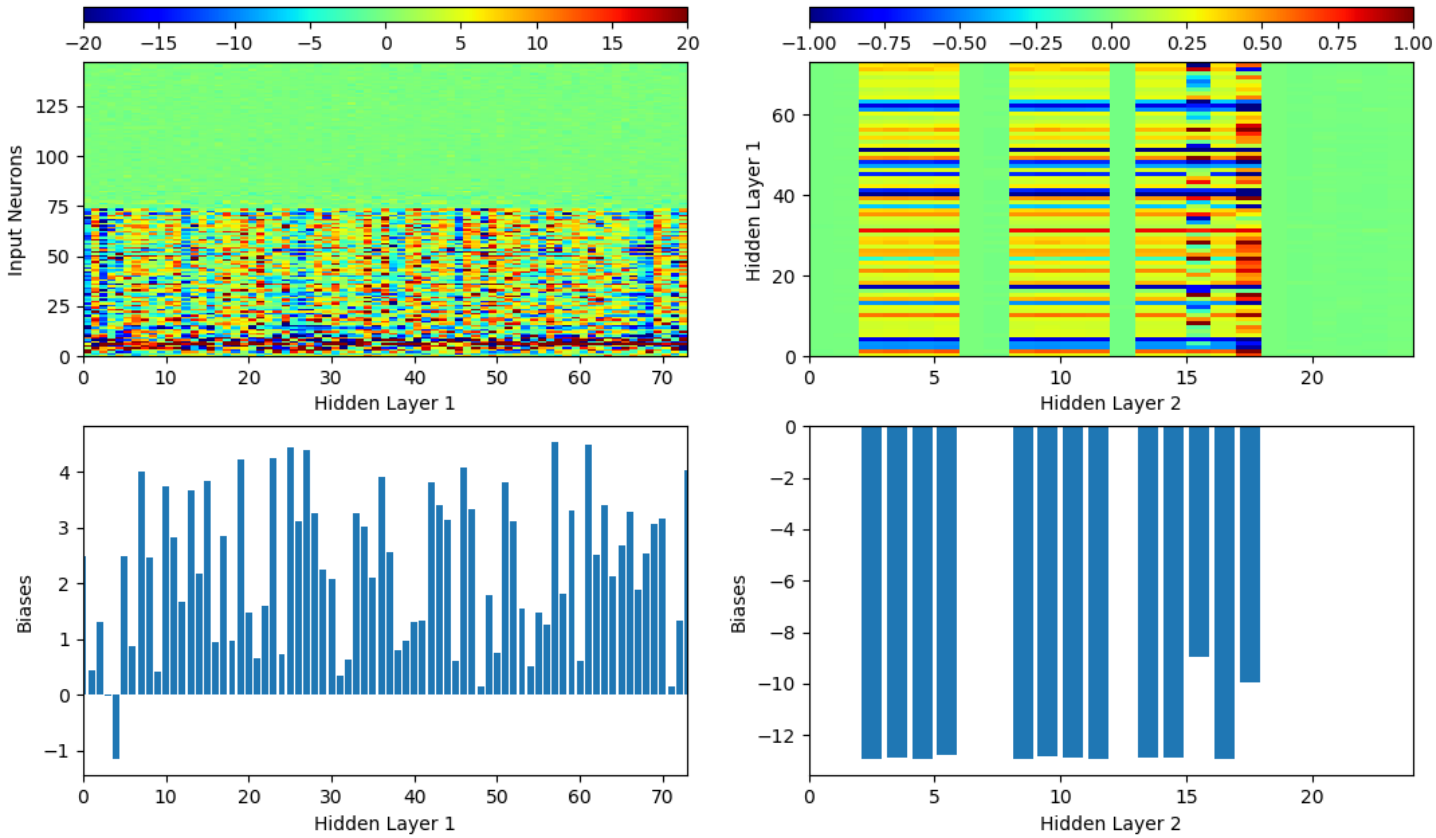

Figure 5.14.: Weights and biases between input layer and second hidden layer; Achieved on database data by usage of the FFT

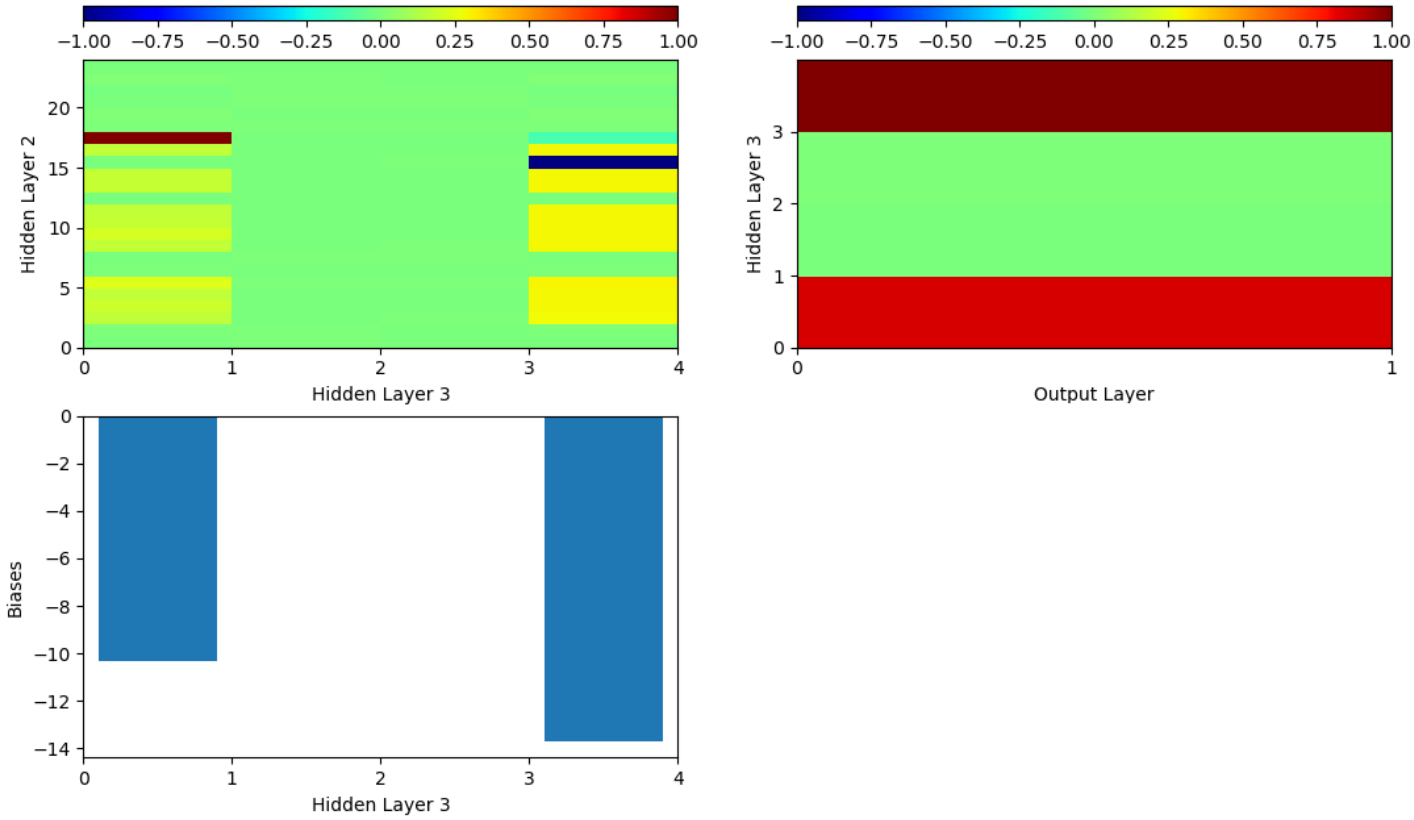

Figure 5.15.: Weights and biases between second hidden layer and output layer; Achieved on database data by usage of the FFT

6. Discussion and Outlook

6.1. Comparison to previous work

As mentioned in Chapter 1.2, this work contines and extends a previous project. This section should give a summary about the differences and improvements compared to the previous thesis [7].

- Software environment
  - Previous: For data collection, preprocessing and training three different environments had to be used. The data collection was done with a special program which stored the collected data into a *txt* file. This file was opend using MATLAB and the preprocessing step was performed. The training of the artificial network was done in python.
  - Now: All data acquisition steps are developed in the Python environment. An own HID communication program was developed for easy data collection, data storage and sensor communication. The preprocessing steps were also done in python. The neuronal network structure was reused, modified and expanded.
- Database handling
  - Previous: Only a few minutes of data per individual were downloaded and used for training and testing. 30 cycles for training and 30 cycles for testing were extracted per individual out of the pre-saved files. The data had to be downloaded from the physionet homepage and selected by hand. The ANN was only able to learn from a limited number of cycles measured for a short time period. The ANN suffers from small data variability and low differences in blood pressure.

  - Now: The python interface can directly download the data from the database. Because of the direct communication it was possible to download the whole set of available data. Over 8h of data per individual was extracted.

- Data quality analysis
  - Previous: The length of the extracted cycles was checked and heart period lengths outside the specified limits were discarded.
  - Now: Additionally a PPG and BP shape inspection was developed for extracting only valid heart periods. A template is generated with represents the average cycle in a specified time range, cycles whose shape differ to much from the template are discarded.
- PALS-2 dataset expansion for own data
  - Previous: 60 samples per one individual are representing the used dataset, 30 were used for training and 30 cycles for testing.
  - Now: By using the cardiovascular unloading technique it was possible to achieve a longer amount of measurements. Data of 16 people for about 20 minutes each were measured. This time range leads to about 1500 collected cycles per individual.
- Feature extraction
  - Previous: After usage of the fast Fourier transformation the amplitude and phase coefficients were fed into the neural network. The zero-padding process was performed after performing the FFT. This means that amplitude and phase coefficients were stored in an array which represents the input vector with a fixed dimension of 300 coefficients. In case of cycles shorter than 150 samples, less than 300 coefficients were calculated and the coefficient vertor's were filled with zeros. This step leads to coefficients representing variable frequency resolution.
  - Now: The cycles are zero-padded before performance of the Fourier transformation. This results in coefficients representing an constant frequency resolution independent of the heart cycle length. Additionally the impact of windowing was investigated and only the single sided amplitude and phase spectrum is used as input for the neuronal network.

- Results
  - Previous: The previous work showed that it is possible to train a network with is meaningful for one individual. The trained weights and biases are only descriptive for the blood pressure of one specific individual; this means that a huge number of reference measurements for every person is necessary.
  - Now: The achieved network is able to estimate blood pressure values of different individuals by usage of the same biases and weights, if heart cycles of the test person were present in the training set.

6.2. Discussion

This work shows that blood pressure estimation by simply using optical measured data is possible and promising at least for persons whose heart cycles are included in the training set. By using the same weights and biases, the blood pressure of different individuals can be estimated without person-specific weight adjustments. The resulting network which was computed from database data is able to estimate the blood pressure for 56 different individuals. If an optimal extended training set could be created, it should be possible to generate a network for estimating blood pressure values for a wide population range. The signal quality for the PPG at the fingertip is much better than for the signal measured on the wrist, due to two reasons: First the fingertip signals are more stable against motion artifacts; Second the proportion of the pulsatile component compared to the DC component, is higher for the fingertip measurement. Nevertheless it was possible to achieve promising results also for data measured via backscattering measurements at the wrist, as they are commonly used in smart-watches for pulse rate measurements. Due to the long time needed for the collection of own measurements, it was not possible to achieve a dataset with similar size compared to the database. Due to some movements of the test subjects also the reference measurement can be disturbed. Deviations from actual blood pressure measured during the reference measurement affect the training process and influence the final result negatively.

As shown in the results of the database and own measured data in Figure 5.3 and 5.8, the estimated pressures can follow the drift of the reference measurements. The RMSE of the trained network for database data is higher than for the own measured data, therefore these results appear better at first glance. For the database data the blood pressure values are spread over a far wider range making the estimation more difficult.

By the usage of neural networks in most cases it is only possible to find a local minimum of the fitting function. By repeating the training process a few times, different minima can be found due to the random initialization of the network weights. In this thesis, the shape of the PPG signal is described by using its FFT coefficients. Due to the limited time

expansion of each heart cycle it may be problematic to describe them with the infinitely extended basis functions sinus and cosinus. For small datasets it was shown that windowing can improve the results, but it was not possible to improve the results compared to not-windowed signals for the whole dataset. For a similar good result significant more training processes were necessary in the case of windowing. Furthermore, it was noticeable that a higher number of epochs was needed to find a good local minimum, even when using the small dataset. Summarized: the usage of windowing makes the training process more unstable.

By using of the Wavelet transformation, the final error and in particular the systolic error values could be decreased. The features used in this case better describe the shape of the PPG signal of a single cardiac cycle, as they can perform temporal localization.

The results of those individuals, whose heart cycles were not included in the training set shown in Figure 5.5, are highly dependent on individual specific properties. The accuracy of the estimation depends on whether people with a similar relationship between blood pressure and PPG signal were included in the training set; and how large the proportion of their heart cycles in the training set was. The following statements can be made regarding the results for individuals of the database data not included in the training set: In particular the course of the diastolic value of test person 1 can be followed well, however, the absolute diastolic pressure was underestimated and the absolute systolic pressure overestimated. The pressure curve of test person 2 is followed well, but the systolic blood pressure in particular is underestimated for this person. The pressures of test person 5 were best estimated, here the estimated pressures can follow the course of the reference, also the estimation of the absolute pressures does not deviate strongly from the reference measurement. The individuals on which the own measurements were carried out, represent only a very limited range of population as their age is between 22-29 years; and probably having similar vessels properties, which thereby provide a poor representation of the population.

The training process itself needs a high computational effort. In comparison, the computational effort to apply the trained weights and biases

on the input data is low. It is very difficult to interpret the weights and biases, due to the non-linear activation function and due to the large number of neurons. To the present state of science the relation between blood pressure and the photoplethysmographic signal is not completely understood. Furthermore, simpler relations between both signals can not be used for blood pressure calculations.

This work shows that it is possible to estimate different persons with the same network if data is present in the training set having similar behaviour. The results for people who are not present in the training set are significantly worse in comparison. The blood pressure is not measured by using physical relationships; there is always the chance to measure individuals with very different pulse shapes compared to the training set. This circumstance should be minimized by collecting more train data of persons with blood pressure curve characteristics as differing as possible. This should be achieved by measuring persons differing in their age, sex and healthiness. Furthermore, it was shown that the use of the Wavelet transformation represents a significant improvement compared to the usage of the Fourier transformation.

6.3. Outlook

By using a wider training set measured from different age groups of people in a clinical setting, it should be possible to achieve equal results for data measured on the wrist as achieved for the fingertip measurements. By adding features to the network like age, gender and sportivity the training process of the network could be additionally supported. The impact of different window functions should be proven more precisely in further research. The usage of the wavelet transformation leads to better results as their limited time expansion may describe the behaviour of the time limited heart cycles better. Since the pressure measurement is not very time critical in most cases, the usage of more successive cycles as input for the FFT calculation leads to a higher frequency resolution and may lead to a reduction of the mean error. In conventional smart-watches, arrays including more LEDs and photo-detectors are used. In this case signals measured on different locations on the wrist are available

simultaneously, which reduces the reliance on corrupted signals during motion artifacts. Due to the easy measurement setup and small package sizes it would be also possible to integrate the LEDs and diodes into hearing aids or headphones. This place seems very suitable for health- and fitness-tracking because it does not affect the user while moving and allows for simple fixation possibilities. The calculation process could be relocated to cell phones, latest devices have integrated AI chips which are optimized for neural network based applications; also TensorFlow has already been presented for mobile scenarios.

Appendix A.

PALS-2 demo board

The PALS-2 demo board includes following parts:

a) PALS-2 The schematic shows the version with external LEDs. On the used board the LEDs were integrated in the package of the optical Infineon ASIC PALS-2.
b) Programming socket
c) PIC Microcontroller
d) Gyroscope and accelerometer LM330 Theoretically it would be possible to measure additional system parameters. They could be used to excluded noisy heart-cycles due to motion artifacts.
e) Pressure sensor Not used so far, could be used for additional pressure measurement or correction of altitude.
f) USB socket
g) Voltage regulator Reg117 Regulates the voltage to 2.7V.

The schematic of the used PALS-2 demo board is shown in figure A.1.

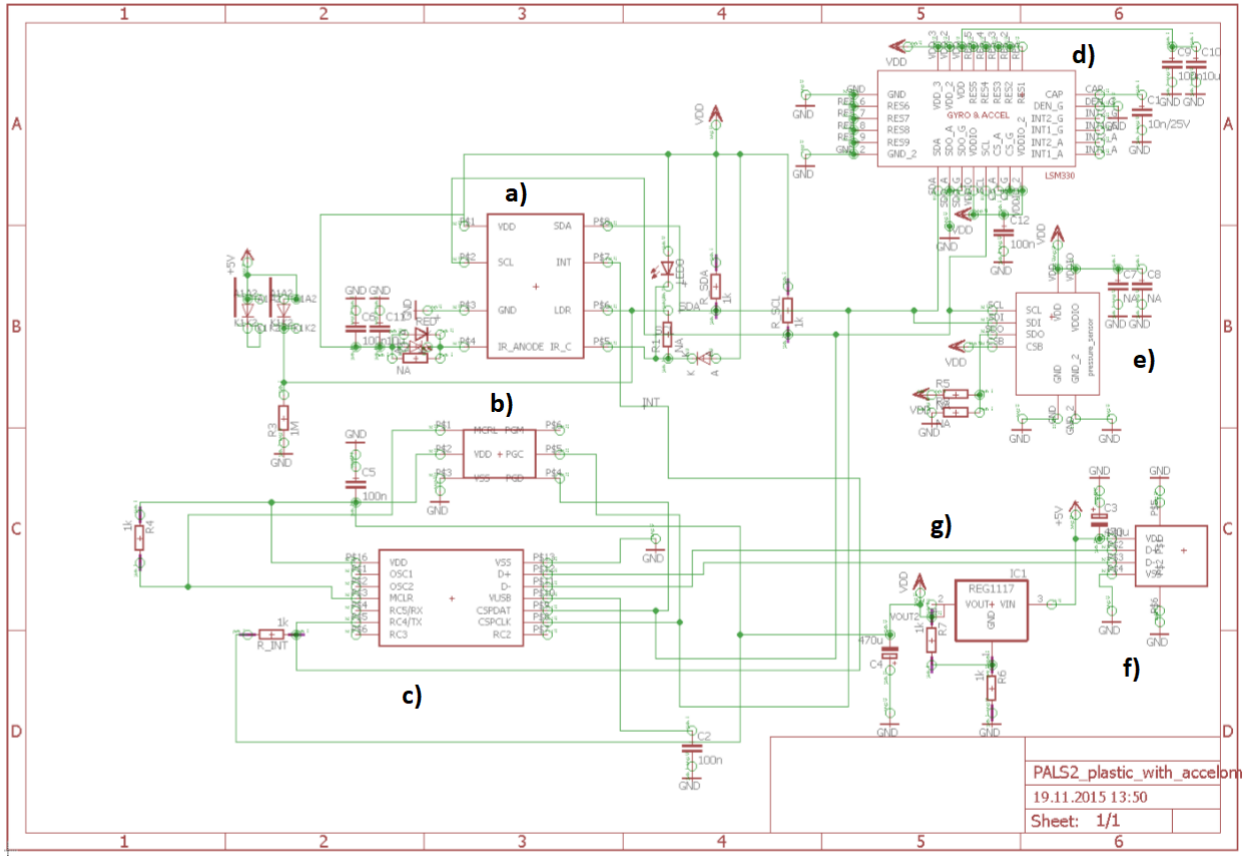

Figure A.1.: Schematic of the used PALS-2 demo board

List of Figures

Bibliography

[1] A. V. Chobanian, G. L. Bakris, H. R. Black, W. C. Cushman, L. A. Green, J. L. Izzo, D. W. Jones, B. J. Materson, S. Oparil, J. T. Wright, E. J. Roccella, and the National High Blood Pressure Education Program Coordinating Committee, *The seventh report of the joint national committee on prevention, detection, evaluation, and treatment of high blood pressure*, JAMA. 289(19):2560-2571, 2003 (cit. on pp. 1, 2, 13, 14).

[2] K. Meigas, R. Kattai, and J. Lass, *Contineous blood pressure monitoring using pulse wave delay*, Conference: Engineering in Medicine and Biology Society IEEE 4, 2001 (cit. on p. 1).

[3] J. Fortin, W. Marte, R. Grüllenberger, A. Hacker, A. Heller, C. Wagner, P. Wach, and F. Skrabal, *Continuous non-invasive blood pressure monitoring using concentrically interlocking control loops*, Comput. Biol. Med 36: 941-957, 2006 (cit. on pp. 1, 27, 28).

[4] A. A. Henning, *Continuous blood pressure measurement using pulse transit time*, A. Somnologie 17: 104, 2013 (cit. on p. 1).

[5] Y. Kurylyak, K. Barbe, F. Lamonaca, D. Grimaldi, and W. V. Moer, *Photoplethysmogram-based blood pressure evaluation using kalman filtering and neural networks*, IEEE MEMEA: 6549729, 2013 (cit. on p. 2).

[6] X. Xing and M. Sun, *Optical blood pressure estimation with photoplethysmography and fft-based neural networks*, Biomed. Opt. Express 261929, 2016 (cit. on pp. 2, 25, 26, 32, 53).

[7] A. Fusco, *A neural network-based approach for continuous blood pressure estimation from photoplethysmography*, Master thesis, Politecnico Milano, 2017 (cit. on pp. 2, 89).

[8] *Physionet database*, https://physionet.org, Accessed on 10.01.2019 (cit. on pp. 4, 33).

[9] W. D. Keidel, H. Bartels, K. Brecht, H. Caspers, and et. al, *Kurzgefasstes lehrbuch der physiologie*, Georg Thieme Verlag Stuttgart, Vol. 5. 1991 (cit. on pp. 7, 12, 13).

[10] *Wiggersdiagram*, en.wikipedia.org/wiki/Wiggersdiagram, Accessed on 12.12.2018 (cit. on pp. 8, 9).

[11] *Figure heart chamber*, www.drugs.com/mcd/heart-failure, Accessed on 18.08.2018 (cit. on p. 9).

[12] G. Thews, E. Mutschler, and P. Vaupel, *Anatomie physiologie pathophysiologie des menschen*, Wissenschaftliche Verlagsgesellschaft Gmbh, Vol. 4. 1991 (cit. on pp. 9, 10).

[13] *Figure windkessel*, www.kidney-international.org, Accessed on 03.09.2018 (cit. on p. 10).

[14] E. Agabiti-Rosei, G. Mancia, M. F. O'Rourke, M. J. Roman, M. E. Safar, H. Smulyan, J.-G. Wang, I. B. Wilkinson, B. Williams, and C. Vlachopoulos, *Central blood pressure measurements and antihypertensive therapy*, Hypertension: 50:154-160, 2007 (cit. on p. 11).

[15] G. Parati, J. E. Ochoa, C. Lombardi, and G. Bilo, *Assessment and management of blood-pressure variability*, Nat. Rev. Cardiol. 10: 143–155, 2013 (cit. on p. 14).

[16] V. Vizbara, A. Sološenko, D. D. Stankevičius, and V. Marozas, *Comparison of green, blue and infrared light in wrist and forehead photoplethysmography*, Conference Biomedical Engineering 2016: 158.129.0.26, 2013 (cit. on pp. 17, 19–21).

[17] *Figure hand (ppg signal acquisition)*, pngimg.com.org, Accessed on 12.10.2018 (cit. on p. 17).

[18] J. Allen, *Photoplethysmography and its application in clinical physiological measurement*, Physiol. Meas. 28: 7, 2007 (cit. on pp. 18, 19, 22).

[19] *Absorption and penetration depth in water and other biological tissues for different wavelengths.* www.intechopen.com/books/frontiers-in-guided-wave-optics-and-optoelectronics/2-m-laser-sources-and-their-possible-applications, Accessed on 14.02.2019 (cit. on p. 19).

[20] M. S. Olufsen, J. T. Ottesen, H. T. Tran, L. M. Ellwein, L. A. Lipsitz, and V. Novak, *Blood pressure and blood ow variation during postural change from sitting to standing: Model development and validation*, J. Appl. Physiol. 99: 1523–1537, 2005 (cit. on pp. 23, 24).

[21] *Figure arterial wall*, teachmeanatomy.info, Accessed on 07.01.2019 (cit. on p. 24).

[22] G. Lopez, M. Shuzom, H. Ushida, K. Hidaka, S. Yangimoto, Y. Imai, A. Kosaka, J.-J. Delaunay, and I. Yamada, *Continuous blood pressure monitoring in daily life*, Journal of Advanced Mechanical Design 4: 09-0412, 2010 (cit. on pp. 28–30).

[23] K. Meigas, R. Kattai, and J. Lass, *Continuous blood pressure monitoring using pulse wave delay*, IEEE 0-7803-7211-5, 2001 (cit. on p. 31).

[24] Y. Kurylyak, F. Lamonaca, and D. Grimaldi, *A neural network-based method for continuous blood pressure estimation from a ppg signal*, IEEE I2MTC: 1091-5281, 2013 (cit. on pp. 31, 32).

[25] I. (P. RFS), *Pals-2 datasheet, version 1.1, m1694a21* (cit. on p. 34).

[26] Q. Li and G. D. Clifford, *Dynamic time warping and machine learning for signal quality assessment of pulsatile signals*, Physiol. Meas. 33: 9, 2012 (cit. on p. 43).

[27] *Scipy.org*, https://docs.scipy.org/doc/numpy/reference, Accessed on 10.01.2019 (cit. on p. 46).

[28] A. Subasi, *Eeg signal classi cation using wavelet feature extraction and a mixture of expert model*, Science Direct 32: 1084-1093, 2007 (cit. on pp. 58–60).

[29] A. Daamouche, L. Hamami, N. Alajlan, and F. Melgani, *A wavelet optimization approach for ecg signal classification*, Biomed. Signal Process. Control 7: 342-349, 2012 (cit. on p. 59).

[30] *Statistics how to*, https://www.statisticshowto.datasciencecentral.com, Accessed on 31.01.2019 (cit. on p. 62).